

# Journal of Intelligent Material Systems and Structures

<http://jim.sagepub.com/>

---

## **Micromechanical Modeling of a Composite Containing Piezoelectric and Shape Memory Alloy Inclusions**

B. Jiang and R. C. Batra

*Journal of Intelligent Material Systems and Structures* 2001 12: 165

DOI: 10.1106/MW7X-YEJK-17XD-GD2N

The online version of this article can be found at:

<http://jim.sagepub.com/content/12/3/165>

---

Published by:



<http://www.sagepublications.com>

**Additional services and information for *Journal of Intelligent Material Systems and Structures* can be found at:**

**Email Alerts:** <http://jim.sagepub.com/cgi/alerts>

**Subscriptions:** <http://jim.sagepub.com/subscriptions>

**Reprints:** <http://www.sagepub.com/journalsReprints.nav>

**Permissions:** <http://www.sagepub.com/journalsPermissions.nav>

**Citations:** <http://jim.sagepub.com/content/12/3/165.refs.html>

>> [Version of Record](#) - Mar 1, 2001

[What is This?](#)

# Micromechanical Modeling of a Composite Containing Piezoelectric and Shape Memory Alloy Inclusions

B. JIANG AND R. C. BATRA\*

*Department of Engineering Science and Mechanics, MC 0219, Virginia Polytechnic Institute and State University, Blacksburg, VA 24061*

**ABSTRACT:** Macroscopic constitutive relations based on the mean-field theory and the Mori–Tanaka method are derived for a 3-phase composite consisting of a polymer matrix and shape memory alloy (SMA) and piezoceramic (PZT) inclusions. Effective moduli are computed for likewise oriented spherical and cylindrical inclusions. Results are also computed for cylindrical PZT and ellipsoidal SMA inclusions. Even though the PZT and the matrix materials are assumed to be linear, the overall response of the composite is nonlinear because of the phase transformations in the SMA inclusions. The 3-phase composite exhibits pyroelectric effects even when none of its constituents is pyroelectric. It is found that the spherical inclusions are more effective than the cylindrical inclusions in the sense that lower values of the average axial stress induce phase transformations in the SMA inclusions, and the maximum principal tensile strain induced in the PZT inclusions is only about 7% of the average axial strain. However, spherical PZT inclusions require a very high value of the electric field to induce any noticeable axial strain in the hybrid composite.

## INTRODUCTION

A “smart composite” should be distinguished from an ordinary composite that is primarily used as a structural material. A smart composite can be tailored to control its shape when subjected to different loads. One or more constituents of a smart composite and hence the composite itself exhibits coupling between at least two of the following four effects: mechanical, thermal, electrical and magnetic. Thus, besides the polymer matrix, other constituents of a smart composite can be a piezoceramic, a shape memory alloy, and/or a magnetostrictive material.

A variety of piezoelectric composite materials, usually called piezocomposites, can be made by combining a piezoelectric ceramic (PZT) with either a non-piezoelectric or a piezoelectric polymer phase; e.g. see the web site (<http://www.matsysinc.com/piezopg.html>) for piezocomposites made by Materials System Inc. Soon after the appearance of barium titanate as a useful piezoelectric ceramic, researchers at the Naval Research Laboratory embedded it in a polymer matrix to make a flexible hydrophone material (Smith, 1989). Pauer (1973) made flexible piezocomposites by combining lead zirconate-titanate ceramic powders with a polymer. Measurements showing the potential for improvement in the performance of naval

hydrophones provided a major impetus to research on piezocomposites (Harrison, 1976).

Piezocomposites have been used as electromechanical and medical ultrasonic imaging transducers. They are more suitable for damage monitoring due to the ease with which their mechanical properties can be tailored, and better impedance matching with that of the host structure. By altering the shape, the size, the volume fraction of the PZTs, and the material of the two phases, a cost-effective piezo-composite with the desired electromechanical coupling constants and impedance can be manufactured.

Newnham et al.’s (1978, 1980) connectivity theory characterized piezocomposites according as the phases are connected in series or in parallel. They also determined the effective properties of these composites. Banno (1983) extended their analyses to discontinuous PZT fibers, and Smith and Auld (1991) to continuous PZT fibers. Smith and Auld (1991) studied the thickness-mode oscillations in thin plates of 1–3 piezocomposites. Such piezocomposites can be treated as a homogeneous medium with new effective material properties so long as the size of the PZT rods and their spacings are sufficiently fine compared with all relevant acoustic wavelengths. Badcock and Birt (2000) have described a technique used to prepare and pole 0–3 piezocomposites, and have also computed their electromechanical properties.

One way to compute effective properties of a piezocomposite is to use the Eshelby tensor for a PZT

\*Author to whom correspondence should be addressed.  
E-mail: rbatra@vt.edu

inclusion in an infinite matrix. Several researchers (e.g. see Deeg (1980), Wang (1992), Dunn and Taya (1993), Chen (1994), Hwang and Yu (1994), Jiang et al. (1997)) have derived Eshelby tensors for piezocomposites. If both the matrix and the inclusions exhibit coupled electromechanical properties, then the Eshelby tensor is expressed in terms of four Green's functions which are difficult to obtain in closed form. However, for a piezocomposite made of piezoelectric inclusions embedded in a non-piezoelectric matrix, only two Green's functions suffice to describe the electroelastic Eshelby tensors (e.g. see Jiang et al. (1997)) and their closed form expressions can be obtained. Benveniste and Dvorak (1990), and Schulgasser (1992) have provided internal consistency relations between the effective moduli of a piezocomposite with continuous PZT fibers. Benveniste (1993a,b) and Benveniste and Dvorak (1990) have generalized the fields concept of Dvorak (1990) to the coupled electroelastic behavior of a piezocomposite. Dunn and Taya (1993) considered ellipsoidal PZT inclusions in a non-piezoelectric elastic matrix and used various micromechanics models to study their electromechanical properties. Dunn (1994) has proved that a piezocomposite can exhibit pyroelectric effects even though neither of its constituents is pyroelectric. He has also estimated the effective thermal expansion and pyroelectric coefficients of a two-phase pyroelectric composite (Dunn, 1993b). The interactions among densely distributed inclusions or inhomogeneities are usually approximated by the Mori-Tanaka (1973) mean field approach. For small concentrations of inclusions, one can use the rule of mixtures to compute the effective properties of a piezocomposite. An alternative to these analytical techniques is to numerically analyze deformations of a representative volume element of a piezocomposite, and determine material properties of an equivalent homogenized system; e.g. see Gabbert et al. (1999).

It is rather well known that PZT actuators supply a small actuation strain but respond quickly to the applied electric field. However, shape memory alloy (SMA) actuators exert significant actuation strains but respond slowly. We take advantage of the beneficial properties of these two materials and study composites made of SMA and PZT inclusions embedded in an elastic matrix. Bidaux et al. (1995), Hamada et al. (1997) and Lee et al. (1997) have developed manufacturing and processing techniques for embedding SMA particles into either an elastic or a ductile matrix. The strengthening effect of SMA wires in an elastic matrix has been studied by Armstrong and Kino (1995), Furuya et al. (1993) and Yamada et al. (1993). The constitutive properties of an SMA composite with an elastic matrix have been studied, amongst others, by Boyd and Lagoudas (1994), Jonnalagadda and Sottos (1995), Sottos et al. (1996), Stalmans et al. (1997), and Sun and Sun (1995).

A micromechanical model of an SMA composite with an elastoplastic matrix has been proposed and analyzed by Cherkaoui et al. (1998) and Song et al. (1999). They have also used a self-consistent scheme to determine the effective properties of an SMA composite in which identical ellipsoidal SMA inclusions are unidirectionally aligned. Taya et al. (1995), Song et al. (1999) and Furuya et al. (1997) used the Eshelby tensor to predict the compressive stress in the matrix material of a SMA composite that was prestrained at the room temperature and then subjected to a temperature increase beyond the austenitic finish temperature. This compressive stress significantly enhanced the tensile properties of a NiTi (Nickel Titanium) SMA fiber/Aluminum matrix composite and of a NiTi SMA fiber/epoxy matrix composite. Other phenomenological macroscopic constitutive models (e.g., Tanaka et al. 1986; Liang and Rogers, 1990; Raniecki et al., 1992; Bekker and Brinson, 1997), and micromechanical models based on the mean field theory (e.g. Patoor et al., 1988; Sun and Hwang, 1993; Boyd and Lagoudas, 1996; Song et al., 1997; Lu and Weng, 1997) have also been proposed. Fischer et al. (1996) and Birman (1997) have reviewed the research on the SMAs.

Because the behavior of a SMA fiber can be modeled as either pseudoelastic (Müller, 1998) or thermo-elastoplastic (Cherkaoui et al., 2000) and it undergoes a phase transformation with a change in temperature, and the PZT fiber's response is electro-elastic, the macroscopic response of a hybrid composite consisting of PZT and SMA fibers in an elastic matrix will be thermo-electro-elasto-plastic. In order to keep the analysis tractable, only infinitesimal deformations are considered. This is reasonable because the PZT is a brittle material with an ultimate tensile strain of about 2%.

Here we use the mean field theory and the Mori-Tanaka method to derive macroscopic constitutive relations of a composite consisting of a polymer matrix and PZT and SMA inclusions. As shown by Dunn (1993b) for a piezocomposite, the three-phase composite studied herein exhibits pyroelectric properties even when none of its constituents is pyroelectric. For cylindrical PZT and SMA inclusions, the axial strain induced by an applied axial electric field decreases as the volume fraction of the PZT inclusions is increased. Results are also computed when PZT and SMA inclusions are spherical.

## CONSTITUTIVE RELATIONS FOR THE MATRIX AND THE INCLUSIONS

A schematic sketch of the problem studied is shown in Figure 1. Figures 2a and 2b respectively depict a composite with all cylindrical and all spherical PZT and SMA inclusions. We presume that the matrix and

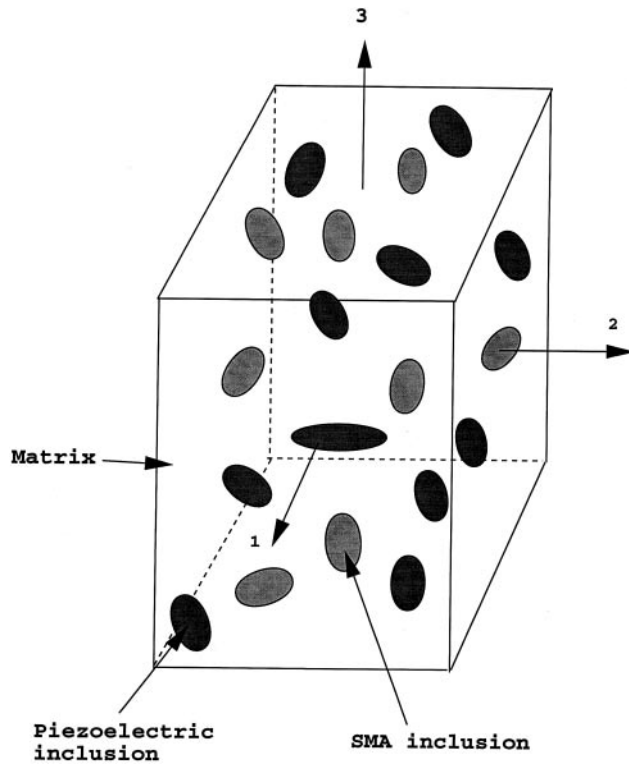


Figure 1. A schematic sketch of the problem studied.

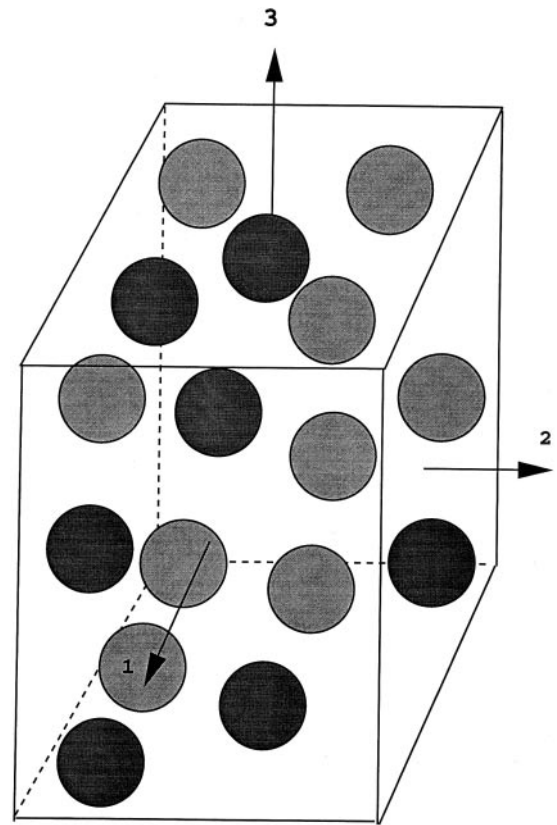


Figure 2b. The hybrid composite with spherical PZT and SMA inclusions.

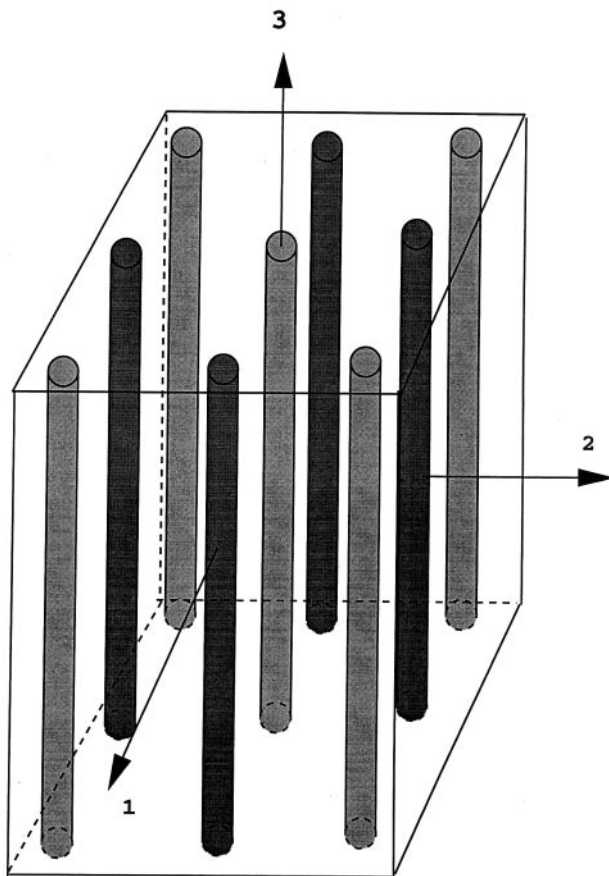


Figure 2a. The hybrid composite with cylindrical PZT and SMA inclusions.

the SMA are nonpiezoelectric, the response of PZT inclusions and the matrix material can be modeled as linear, the deformations are infinitesimal, the values of the material parameters of the matrix, the PZT and the SMA are independent of the time and the temperature, the inclusions are perfectly bonded to the matrix, and the temperature of the composite is always uniform. In rectangular Cartesian coordinates, the constitutive relations for the matrix, the PZT inclusions and the SMA are

$$\sigma_{ij} = C_{ijkl}^M \epsilon_{kl} - \lambda_{ij}^M \theta, \quad D_i = k_{ij}^M E_j + p_i^M \theta, \quad (1)$$

for the matrix,

$$\sigma_{ij} = C_{ijkl}^P \epsilon_{kl} - e_{kij}^P E_k - \lambda_{ij}^P \theta, \quad D_i = e_{ijk}^P \epsilon_{jk} + k_{ij}^P E_j + p_i^P \theta, \quad (2)$$

for the PZT,

$$\sigma_{ij} = C_{ijkl}^S (\epsilon_{kl} - \epsilon_{kl}^{tr}) - \lambda_{ij}^S \theta, \quad D_i = k_{ij}^S E_j + p_i^S \theta, \quad (3)$$

for the SMA.

Here  $\sigma_{ij}$  is the stress tensor,  $\epsilon_{ij}$  the strain tensor appropriate for infinitesimal deformations,  $\epsilon_{ij}^{tr}$  the transformation strain in the SMA,  $E_i$  the electric field,  $\theta$  the change in the temperature from that in the reference configuration,  $C_{ijkl} = C_{klij} = C_{ijlk}$  are the elasticities,  $\lambda_{ij}$  the stress-temperature moduli,  $k_{ij}$  the dielectric constants,  $p_i$  the pyroelectric coefficients, and  $e_{ijk}$  the

piezoelectric constants. Superscripts  $M$  and  $P$  signify, respectively, quantities for the matrix and the PZT.

We note that two phases, namely austenite and martensite, can coexist in the SMA. The material properties of an SMA can be determined from those of the austenite and the martensite phases by using either the mean field theory or the energy equivalence method or the rule of mixtures. Following Boyd and Lagoudas (1994) we assume that the rule of mixtures approximates well the overall properties of an SMA. Thus

$$C_{ijkl}^S = (1 - \xi)C_{ijkl}^a + \xi C_{ijkl}^m \quad (4)$$

and similar relations hold for  $k_{ij}^S$ ,  $\alpha_{ij}^S$  and  $p_i^S$ , where  $\alpha_{ij}^S$  are the coefficients of thermal expansion of the SMA. In Equation (4), superscripts  $S$ ,  $a$  and  $m$  signify quantities for an SMA, austenite and martensite respectively. The volume fraction  $\xi$  of the martensite phase is given by

$$\xi = \frac{\epsilon_e^{tr}}{\epsilon_{\max}^{tr}}, \quad \epsilon_e^{tr} = \left( \frac{2}{3} \epsilon_{ij}^{tr} \epsilon_{ij}^{tr} \right)^{1/2}, \quad (5)$$

where  $\epsilon_{ij}^{tr}$  is the transformation induced strain in the SMA, and  $\epsilon_{\max}^{tr}$  is the maximum value of the equivalent transformation strain,  $\epsilon_e^{tr}$ , which is regarded as a material property (Song et al., 1999). We note that  $\lambda_{ij}^S = C_{ijkl}^S \alpha_{kl}^S$ .

## EFFECTIVE MODULI OF THE HYBRID COMPOSITE

Let  $\Omega_M$ ,  $\Omega_P$  and  $\Omega_S$  denote respectively the regions occupied by the matrix, the PZT inclusions and the SMA inclusions. Constitutive relations (1), (2) and (3) can be written as

$$\begin{aligned} \sigma_{ij}(\mathbf{x}) &= C_{ijkl}(\mathbf{x})\epsilon_{kl}(\mathbf{x}) - e_{kij}(\mathbf{x})E_k(\mathbf{x}) - \lambda_{ij}(\mathbf{x})\theta(\mathbf{x}) + \sigma_{ij}^*(\mathbf{x}), \\ D_i(\mathbf{x}) &= e_{ijk}(\mathbf{x})\epsilon_{jk}(\mathbf{x}) + k_{ij}(\mathbf{x})E_j(\mathbf{x}) + p_i(\mathbf{x})\theta(\mathbf{x}). \end{aligned} \quad (6)$$

If  $\mathbf{x} \in \Omega_M$ ,  $\Omega_P$  or  $\Omega_S$ , the material parameters in (6) are, respectively, those for the matrix, the PZT and the SMA. When  $\mathbf{x} \in \Omega_P$  or  $\Omega_M$ ,  $\sigma_{ij}^*(\mathbf{x}) = 0$ . However, for  $\mathbf{x} \in \Omega_S$ ,  $\sigma_{ij}^*(\mathbf{x}) = -C_{ijkl}^S \epsilon_{kl}^{tr}$ . This essentially smears the austenite/martensite together into a homogeneous medium. A more sophisticated treatment would have been to consider the martensite moduli and the transformation strain to compute the transformation induced stress.

We assume that the hybrid composite can be regarded as statistically homogeneous, and the transformation strains in the SMA can also be assumed to be statistically homogeneous. The effective thermo-electro-elastic

constants of the hybrid composite are defined by the relations

$$\begin{aligned} \bar{\sigma}_{ij} &= \bar{C}_{ijkl}\bar{\epsilon}_{kl} - \bar{e}_{kij}\bar{E}_k - \bar{\lambda}_{ij}\bar{\theta} + \bar{\sigma}_{ij}^*, \\ \bar{D}_i &= \bar{e}_{ijk}\bar{\epsilon}_{jk} + \bar{k}_{ij}\bar{E}_j + \bar{p}_i\bar{\theta} + \bar{D}_i^{*\epsilon}, \end{aligned} \quad (7)$$

where  $\bar{\sigma}_{ij}^*$  and  $\bar{D}_i^{*\epsilon}$  are, respectively, the residual stress and the residual electric displacement caused by the transformation strain, and an overbar on a quantity denotes its volume average over the entire domain  $\Omega$  of the hybrid composite, or over the  $r$ th phase  $\Omega_r$  ( $r = P, S$  or  $M$ ) as is appropriate. For example

$$\bar{\theta} = \langle \theta \rangle = \frac{1}{\Omega} \int_{\Omega} \theta d\Omega. \quad (8)$$

Let displacements corresponding to the uniform strain  $\epsilon_{ij}^0$ , the electric potential corresponding to the uniform electric field  $E_i^0$  and the uniform temperature  $\theta^0$  be applied on the boundary  $\partial\Omega$  of  $\Omega$ . Then under equilibrium conditions, the fields within  $\Omega$  are given by

$$\bar{\epsilon}_{ij}(\mathbf{x}) = \epsilon_{ij}^0, \quad \bar{E}_i(\mathbf{x}) = E_i^0, \quad \bar{\theta}(\mathbf{x}) = \theta^0. \quad (9)$$

However, in general

$$\begin{aligned} \epsilon_{ij}(\mathbf{x}) &= L_{ijkl}(\mathbf{x})\epsilon_{kl}^0 + N_{ijk}(\mathbf{x})E_k^0 + R_{ij}(\mathbf{x})\theta^0 + \epsilon_{ij}^{**}(\mathbf{x}), \\ E_i(\mathbf{x}) &= P_{ijk}(\mathbf{x})\epsilon_{jk}^0 + Q_{ij}(\mathbf{x})E_j^0 + J_i(\mathbf{x})\theta^0 + E_i^{**}(\mathbf{x}), \end{aligned} \quad (10)$$

where the influence functions  $\mathbf{L}$ ,  $\mathbf{N}$ ,  $\mathbf{R}$ ,  $\mathbf{P}$ ,  $\mathbf{Q}$  and  $\mathbf{J}$ , and the concentration tensors  $\epsilon_{ij}^{**}$  and  $E_i^{**}$  obtained by the Mori–Tanaka method are given in the Appendix. Substitution from (10) into (9) and exploiting the fact that the resulting equations must hold for all choices of  $\epsilon_{ij}^0$ ,  $E_i^0$  and  $\theta^0$ , we obtain

$$\begin{aligned} \langle L_{ijkl}(\mathbf{x}) \rangle &= I_{ijkl}, \quad \langle \mathbf{N}(\mathbf{x}) \rangle = \mathbf{0}, \quad \langle \mathbf{R}(\mathbf{x}) \rangle = \mathbf{0}, \quad \langle \epsilon^{**}(\mathbf{x}) \rangle = \mathbf{0}, \\ \langle \mathbf{P}(\mathbf{x}) \rangle &= \mathbf{0}, \quad \langle Q_{ij}(\mathbf{x}) \rangle = \delta_{ij}, \quad \langle \mathbf{J}(\mathbf{x}) \rangle = \mathbf{0}, \quad \langle \mathbf{E}^{**}(\mathbf{x}) \rangle = \mathbf{0}, \end{aligned} \quad (11)$$

where  $I_{ijkl} = (\delta_{ik}\delta_{jl} + \delta_{il}\delta_{jk})/2$ , and  $\delta_{ij}$  is the Kronecker delta. From Equations (6), (7), (10) and (11) we conclude that

$$\begin{aligned} \bar{C}_{ijkl} &= \langle C_{ijmn}L_{mnkl} - e_{mij}P_{mkl} \rangle, \\ \bar{e}_{kij} &= \langle e_{mij}Q_{mk} - C_{ijmn}N_{mnk} \rangle, \\ \bar{k}_{ij} &= \langle e_{ilm}N_{lmj} + k_{il}Q_{lj} \rangle, \\ \bar{\lambda}_{ij} &= \langle \lambda_{ij} - C_{ijkl}R_{kl} + e_{kij}J_k \rangle, \\ \bar{p}_i &= \langle p_i + e_{ijk}R_{jk} + k_{ij}J_j \rangle, \\ \bar{\sigma}_{ij}^* &= \langle \sigma_{ij}^* + C_{ijkl}\epsilon_{kl}^{**} - e_{kij}E_k^{**} \rangle, \\ \bar{D}_i^{*\epsilon} &= \langle e_{ijk}\epsilon_{jk}^{**} + k_{ij}E_j^{**} \rangle. \end{aligned} \quad (12)$$

The influence functions must satisfy the consistency condition

$$\langle Q_{ij}e_{ilm} - N_{pqj}C_{pqlm} \rangle = \langle e_{jpq}L_{pqlm} + k_{jp}P_{plm} \rangle. \quad (13)$$

Benveniste (1993) derived Equation (13) by using the principle of virtual work. Substitution for the material properties of the matrix, the piezoelectric inclusions, and the SMA inclusions into (12) gives the following expressions for the effective properties of the hybrid composite.

$$\begin{aligned} \bar{C}_{ijkl} &= \Phi_{ijmn}^1 L_{mnkl}^M + \Phi_{ijm}^2 P_{mkl}^M, \\ \bar{e}_{kij} &= \Phi_{kmn}^3 L_{mnij}^M + \Phi_{km}^4 P_{mij}^M, \\ \bar{k}_{ij} &= \Phi_{ilm}^3 N_{lmj}^M + \Phi_{im}^4 Q_{mj}^M, \\ \bar{\lambda}_{ij} &= \Psi_{ij}^1 - \Phi_{ijmn}^1 R_{mn}^M - \Phi_{ijm}^2 J_m^M, \\ \bar{p}_i &= \Psi_i^2 + \Phi_{imn}^3 R_{mn}^M + \Phi_{ij}^4 J_j^M, \\ \bar{\sigma}_{ij}^* &= \Gamma_{ij}^1 + \Phi_{ijmn}^1 \epsilon_{mn}^{**M} + \Phi_{ijm}^2 E_m^{**M}, \\ \bar{D}_i^{*\epsilon} &= \Phi_{ikl}^3 \epsilon_{kl}^{**M} + \Phi_{ij}^4 E_j^{**M}, \end{aligned} \quad (14)$$

where

$$\begin{aligned} \Phi_{ijkl}^1 &= f_M \langle C_{ijkl}^M \rangle_M + f_S \langle C_{ijpq}^S H_{pqkl}^{1S} \rangle_S \\ &\quad + f_P \langle C_{ijpq}^P H_{pqkl}^{1P} - e_{mij}^P H_{mkl}^{3P} \rangle_P, \\ \Phi_{ijk}^2 &= f_P \langle C_{ijmn}^P H_{mnk}^{2P} - e_{mij}^P H_{mk}^{4P} \rangle_P, \\ \Phi_{ilm}^3 &= f_P \langle e_{ijk}^P H_{jklm}^{1P} + k_{ij}^P H_{jlm}^{3P} \rangle_P, \\ \Phi_{ij}^4 &= f_M \langle k_{ij}^M \rangle_M + f_S \langle k_{il}^S H_{ij}^{4S} \rangle_S + f_P \langle e_{ilm}^P H_{lmj}^{2P} + k_{il}^P H_{lj}^{4P} \rangle_P, \\ \Psi_{ij}^1 &= \sum_{r=M,P,S} f_r \langle \lambda_{ij}^r \rangle_r - f_S \langle C_{ijlm}^S F_{lm}^{1S} \rangle_S \\ &\quad - f_P \langle C_{ijlm}^P F_{lm}^{1P} - e_{ij}^P F_l^{2P} \rangle_P, \\ \Psi_i^2 &= \sum_{r=M,P,S} f_r \langle p_i^r \rangle_r + f_S \langle k_{ij}^S F_j^{2S} \rangle_S + f_P \langle e_{ijk}^P F_{jk}^{1P} + k_{ij}^P F_j^{2P} \rangle_P, \\ \Gamma_{ij}^1 &= f_S \langle C_{ijkl}^S (S_{klmn}^{1S} - I_{klmn}) \epsilon_{mn}^{tr} \rangle_S. \end{aligned} \quad (15)$$

Here  $f_M$ ,  $f_P$  and  $f_S$  equal, respectively, the total volume fractions of the matrix, the PZT inclusions and the SMA inclusions. Expressions for the thermoelastic Eshelby tensors  $\mathbf{H}^1$ ,  $\mathbf{F}^1$  etc. are given in the Appendix; the added superscripts  $M$ ,  $P$  and  $S$  signify quantities for the matrix, the PZT and the SMA respectively.

The constitutive relations (7)<sub>1</sub> (i.e. the first of Equations (7)) can be solved for  $\bar{\epsilon}_{ij}$  in terms of  $\bar{\sigma}_{ij}$ ,  $\bar{E}_i$ ,  $\bar{\theta}$  and  $\bar{\sigma}_{ij}^*$  and the result substituted into Equation (7)<sub>2</sub> to obtain  $\bar{\epsilon}_{ij}$  and  $\bar{D}_i$  as a linear function of the  $\bar{\sigma}_{ij}$ ,  $\bar{E}_i$ , and  $\bar{\theta}$ .

Equation (14)<sub>5</sub> implies that  $\bar{\mathbf{p}}$  need not vanish even when  $\mathbf{p}^M = \mathbf{p}^P = \mathbf{p}^S = \mathbf{0}$ . That is, the hybrid composite

may exhibit the pyroelectric effect even when none of its constituents is pyroelectric; a similar result was obtained by Dunn (1993b) for a composite made of PZT inclusions and an elastic matrix. This is because thermal stresses caused by a change in the temperature of the hybrid composite induce an electric field in the PZT inclusions which gives rise to the effective or overall pyroelectric effect. However, when  $\lambda^M = \lambda^P = \lambda^S$ , then the hybrid composite exhibits no pyroelectric effect.

Even though there is no residual electric displacement in the PZT inclusions, the residual electric displacement of the hybrid composite is nonzero due to the eigen-strain in the SMA inclusions. The effective thermo-electroelastic moduli  $\bar{\mathbf{C}}$ ,  $\bar{\mathbf{e}}$  and  $\bar{\mathbf{k}}$  of the hybrid composite are related to  $\mathbf{C}^r$ ,  $\mathbf{e}^r$  and  $\mathbf{k}^r$  ( $r = M, P, S$ ) and the shapes and the orientations of the inclusions, but are independent of  $\lambda^r$  and  $\mathbf{p}^r$ . However,  $\bar{\lambda}$  and  $\bar{\mathbf{p}}$  of the hybrid composite depend upon all of the material properties of its constituents and also on its microstructure. If the material properties of the austenite and the martensite are the same, we find that the effective thermo-electroelastic moduli are independent of the volume fraction  $\xi$  of the martensite but the residual stresses and the residual electric displacement vary with  $\xi$ .

## PHASE TRANSFORMATIONS IN THE SMA

The evolution of the volume fraction,  $\xi$ , of the martensite depends upon the state of stress and temperature in the SMA. The stress state in the SMA is given by

$$\sigma_{ij}^S = U_{ijkl}^S \sigma_{kl}^0 + V_{ijk}^S E_k^0 + W_{ij}^S \theta^0 + \sigma_{ij}^{**S}, \quad (16)$$

where

$$\begin{aligned} U_{ijkl}^S &= H_{ijmn}^{5S} L_{mnkl}^\sigma, \quad V_{ijk}^S = H_{ijmn}^{5S} N_{mnk}^\sigma, \\ W_{ij}^S &= F_{ij}^{3S} + H_{ijmn}^{5S} R_{mn}^\sigma, \\ \sigma_{ij}^{**S} &= S_{ijkl}^{5S} \epsilon_{kl}^{tr} - f_S U_{ijkl}^S \langle S_{klmn}^{5S} \epsilon_{mn}^{tr} \rangle_S, \end{aligned} \quad (17)$$

and matrices  $\mathbf{H}^{5S}$ ,  $\mathbf{S}^{5S}$ ,  $\mathbf{L}^\sigma$ ,  $\mathbf{N}^\sigma$ ,  $\mathbf{F}^{3S}$  and  $\mathbf{R}^\sigma$  are defined in the Appendix. When the orientation of each SMA inclusion is the same, we have

$$\sigma_{ij}^{**S} = Y_{ijkl}^S \epsilon_{kl}^{tr}, \quad (18)$$

where

$$Y_{ijkl}^S = (I_{ijmn} - f_S U_{ijmn}^S) S_{mnkl}^{5S}, \quad (19)$$

and the matrix  $S^{5S}$  is defined in the Appendix. Let  $\dot{\Sigma}_{ij}^0$  equal the change of the stress in the SMA inclusions due to the variation of the applied fields  $\sigma^0$ ,  $\mathbf{E}^0$  and  $\theta^0$ , and  $\dot{\Sigma}_{ij}^\xi$  the change of the stress in the SMA due to the

evolution of the martensite phase. That is,

$$\begin{aligned} \dot{\Sigma}_{ij}^0 &= U_{ijkl}^S \dot{\sigma}_{kl}^0 + V_{ijk}^S \dot{E}_k^0 + W_{ij}^S \dot{\theta}^0, \\ \dot{\Sigma}_{ij}^\xi &= \left( \frac{\partial U_{ijkl}^S}{\partial \xi} \sigma_{kl}^0 + \frac{\partial V_{ijk}^S}{\partial \xi} E_k^0 + \frac{\partial W_{ij}^S}{\partial \xi} \theta^0 + \frac{\partial Y_{ijkl}^S}{\partial \xi} \epsilon_{kl}^{tr} \right) \dot{\xi} \\ &+ Y_{ijkl}^S \epsilon_{kl}^{tr}, \end{aligned} \quad (20)$$

where a superimposed dot indicates a change or an increment in the quantity. Using Equation (5)<sub>1</sub>, one can express  $\dot{\xi}$  in terms of  $\epsilon_{ij}^{tr}$ . Following Boyd and Lagoudas (1994), Song et al. (1999) and Cherkaoui et al. (2000), we assume that

$$\dot{\epsilon}^{tr} = \begin{cases} \dot{\Lambda}^S \mathbf{s} & \text{for the forward transformation,} \\ \dot{\Lambda}^{re} \epsilon^{tr} & \text{for the reverse transformation,} \end{cases} \quad (21)$$

where  $\dot{\Lambda}$  and  $\dot{\Lambda}^{re}$  are proportionality factors to be determined from the consistency condition, and  $\mathbf{s}$  is the deviatoric stress tensor. Note that  $\dot{\Lambda}$  and  $\dot{\Lambda}^{re}$  have different dimensions. Evaluating the incremental change in different quantities from Equation (16) and using Equations (5), (20) and (21) we arrive at

$$\dot{\Lambda} = - \frac{s_{ij}^S \dot{\Sigma}_{ij}^0 - (2/3) s_e (\partial s_e^S / \partial \theta) \dot{\theta}^0}{s_{ij}^S \left[ (2/3) \epsilon_{max}^{tr} \epsilon_e^{tr} \dot{\Sigma}_{ij}^\xi (\epsilon_{kl}^{tr} s_{kl}^S) + Y_{ijkl}^S s_{kl}^S \right]} \quad (22)$$

for the forward (austenite  $\rightarrow$  martensite) and

$$\dot{\Lambda}^{re} = - \frac{s_{ij}^S \dot{\Sigma}_{ij}^0 - (2/3) s_e (\partial s_e^S / \partial \theta) \dot{\theta}^0}{s_{ij}^S \left[ (\epsilon_e^{tr} / \epsilon_{max}^{tr}) \dot{\Sigma}_{ij}^\xi + Y_{ijkl}^S \epsilon_{kl}^{tr} \right]} \quad (23)$$

for the reverse (martensite  $\rightarrow$  austenite) transformation. Here

$$s_e = ((3/2) s_{ij} s_{ij})^{1/2} \quad (24)$$

is the equivalent or the effective or the von Mises stress, and the forward transformation initiates when  $s_e^S = s_e^{fS}(\theta)$  and the reverse transformation begins when  $s_e^S = s_e^{rS}(\theta)$ . Note that  $s_e^{fS}(\theta)$  and  $s_e^{rS}(\theta)$  are temperature dependent material parameters. However, here the temperature of the composite is assumed to be uniform and constant.

### COMPARISON OF RESULTS WITH EXPERIMENTAL FINDINGS AND PREDICTIONS FROM OTHER MODELS

To the authors' knowledge, there is no experimental data available for the 3-phase composite studied herein. Therefore, we first compare computed values of some of

the effective moduli of an 1–3 piezocomposite with the experimental results of Chan and Unsworth (1989). Subsequently, for a composite made of an elastic matrix and cylindrical SMA inclusions aligned along the  $x_3$ -axis, we compare our results with those reported by Lagoudas et al. (1994).

Figures 3a and 3b depict the experimental and the computed values of the effective piezoelectric constant  $\tilde{d}_{333}$ , the effective dielectric constant  $\tilde{k}_{33}$ , the

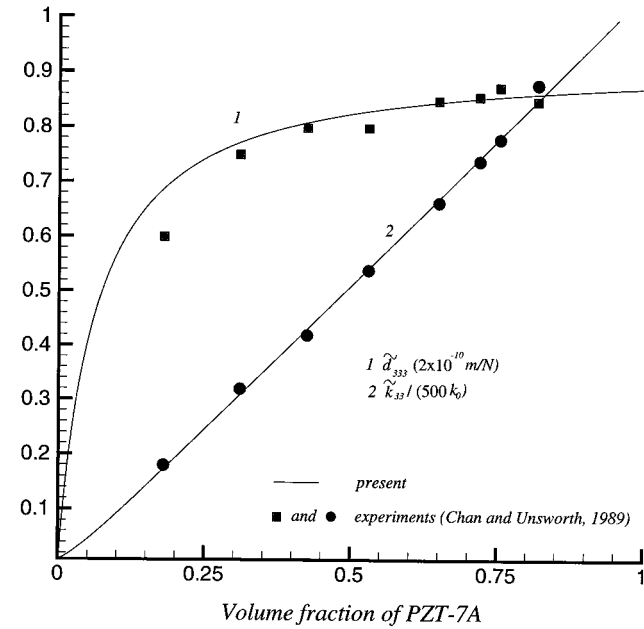


Figure 3a. Comparison of the computed and the experimental values of  $d_{333}$  and  $k_{33}$  for an 1–3 piezocomposite.

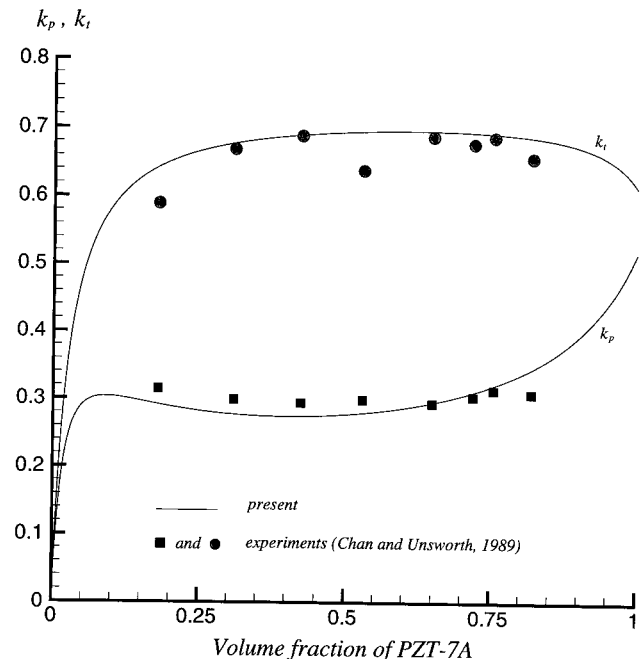


Figure 3b. Comparison of the computed and the experimental values of  $k_p$  and  $k_t$  for an 1–3 piezocomposite.

effective thickness coupling constant  $k_t$ , and the effective planar coupling constant  $k_p$  for the 1–3 piezocomposite made of PZT7A cylindrical wires embedded in an Araldite D material. The matrix is modeled as an isotropic material and the PZT7A as transversely isotropic with the axis of polarization coincident with the  $x_3$ -axis. Values of material constants for these two materials are given in Chan and Unsworth (1989). The planar moduli  $k_p$  and  $k_t$  are given by

$$k_p = \sqrt{\frac{2(\tilde{d}_{311})^2}{\tilde{k}_{33}(\tilde{M}_{1111} + \tilde{M}_{1122})}}, \quad k_t = \frac{B - Ak_p}{\sqrt{1 - A^2}\sqrt{1 - k_p^2}},$$

where

$$A = \sqrt{\frac{2(\tilde{M}_{1133})^2}{\tilde{M}_{3333}(\tilde{M}_{1111} + \tilde{M}_{1122})}}, \quad B = \sqrt{\frac{(\tilde{d}_{333})^2}{\tilde{k}_{33}\tilde{M}_{333}}}$$

It is clear that the two sets of results agree well with each other. With an increase in the volume fraction of the PZT7A inclusions,  $\tilde{k}_{33}$  increases linearly and  $k_t$  appears to approach a saturation value. The slope of the  $\tilde{d}_{333}$  vs.  $f^P$  curve decreases with an increase in the value of  $f^P$  and is nearly a constant for  $f^P \geq 0.5$ .

For values of material parameters of the matrix and the SMA listed in Lagoudas et al. (1994) and both materials modeled as isotropic, Figure 4 depicts the axial stress,  $\sigma_{33}$ , vs. the axial strain curves for a rectangular

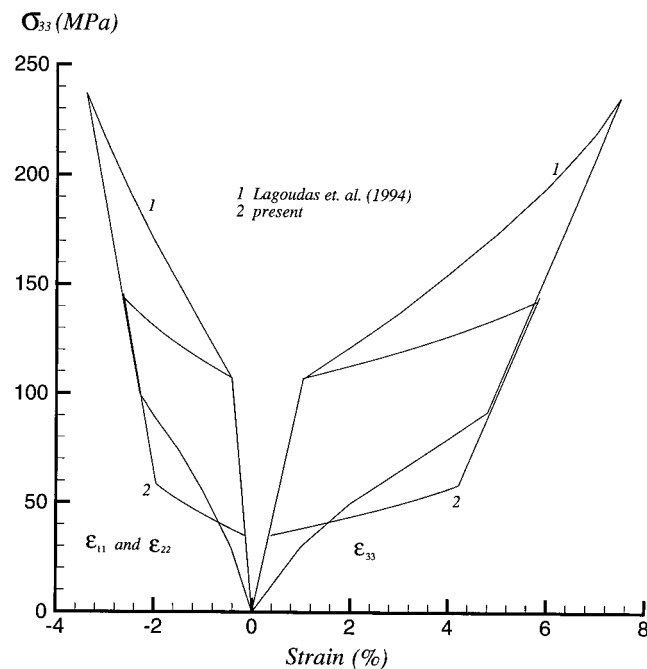


**Figure 4.** Comparison of the axial stress vs. axial and lateral strains for a uniaxially loaded composite comprised of an elastic matrix and cylindrical SMA inclusions.

block of the composite material loaded in the  $x_3$ -direction only. The cylindrical SMA inclusions with  $f^S = 0.30$  are aligned along the  $x_3$ -axis. Subsequent to the initiation of the phase transformation in the SMA, our results differ from those of Lagoudas et al. (1994) because they account for work hardening of the SMA and we do not. The values of the effective Young's modulus and the effective Poisson's ratio computed by the two models essentially coincide with each other.

## RESULTS AND DISCUSSION

We compute and discuss results for a hybrid composite comprised of a polymer matrix, BaTiO<sub>3</sub> as the PZT material and the SMA made of a NiTi alloy. Nonzero values of material parameters are listed in Table 1. We model the polymer matrix and the SMA as isotropic, and the PZT as transversely isotropic with the  $x_3$ -axis as the axis of polarization and hence of transverse isotropy. We investigate the following three cases: (i) identically oriented cylindrical PZT and SMA inclusions, (ii) identically aligned spherical PZT and SMA inclusions, and (iii) cylindrical PZT and ellipsoidal SMA inclusions. In each case, the temperature of the composite stays uniform at 10°C which is above the austenite finish temperature. Each constituent and the body is assumed to be stress free in the reference configuration at 10°C.

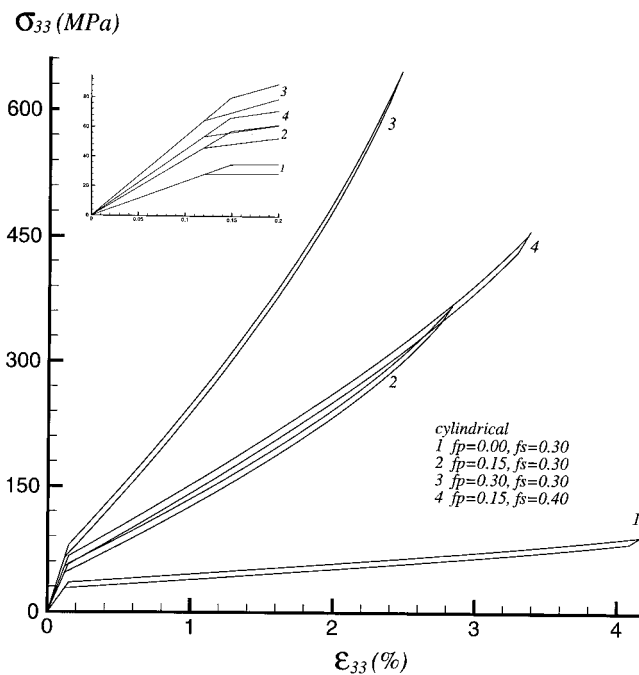
### Axial Stress–Axial Strain Relations

Figures 5 and 6 exhibit respectively, the variation of the axial strain with the axial stress for the hybrid composite containing cylindrical and spherical inclusions, loaded only along the  $x_3$ -axis, and zero electric field and no temperature change applied on the bounding surfaces. Prior to the initiation of the forward transformation in the SMA, the stress–strain relationship for the composite is linear and the macroscopic axial strain is quite small. When the equivalent stress  $s_e^S(\theta)$  in the SMA reaches 100 MPa, the value required for the initiation of the forward transformation in the SMA, the forward transformation ensues in the SMA inclusions and the macroscopic strain of the composite increases noticeably. For both spherical and cylindrical inclusions, the forward transformation in the SMA inclusions initiates at a value of the applied axial stress which is considerably smaller than that required to initiate the forward transformation in the pure SMA. This is because the values of the elasticities of the polymer matrix are at least an order of magnitude lower than those of the inclusions. Consequently, in order for the axial strain to be the same in the matrix and the inclusions, inclusions take up a larger portion of the applied axial tractions. This also explains the increase in

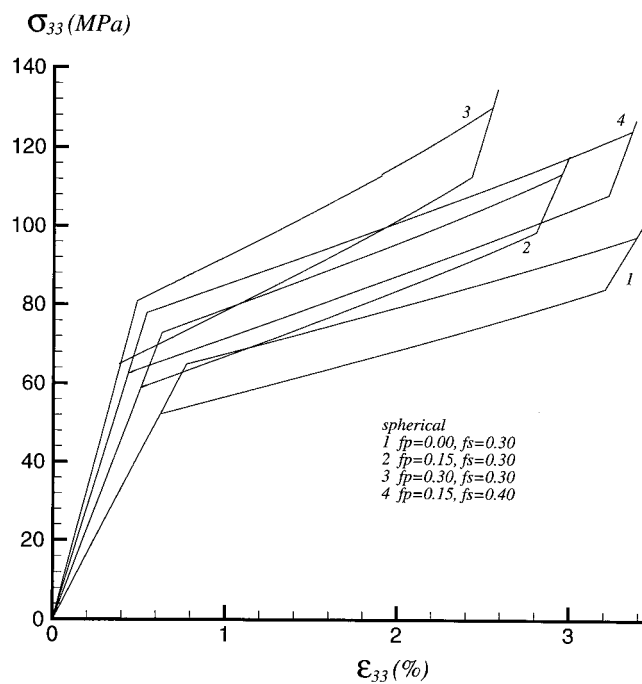
**Table 1. Material parameters of the three constituents of the hybrid composite.**

	Polymer <sup>a</sup>	BaTiO <sub>2</sub> <sup>b</sup>	Austenite <sup>b</sup>	Martensite <sup>b</sup>
C <sub>1111</sub> (Gpa)	8.0	150.0	143.57	56.36
C <sub>1122</sub> (Gpa)	4.4	66.0	95.71	37.57
C <sub>1133</sub> (Gpa)	4.4	66.0	95.71	37.57
C <sub>3333</sub> (Gpa)	8.0	146.0	143.57	56.36
C <sub>1313</sub> (Gpa)	1.8	44.0	23.93	9.39
e <sub>311</sub> (C/m <sup>2</sup> )	0	-4.35	0	0
e <sub>333</sub> (C/m <sup>2</sup> )	0	17.5	0	0
e <sub>131</sub> (C/m <sup>2</sup> )	0	11.4	0	0
k <sub>11</sub> /k <sub>0</sub>	4.0	1115.0	0	0
k <sub>33</sub> /k <sub>0</sub>	4.0	1260.0	0	0
λ <sub>-11</sub> (MPa/°C)	1.008	1.974	3.685	0.8679
λ <sub>33</sub> (MPa/°C)	1.008	1.471	3.685	0.8679
p <sub>3</sub> (10 <sup>-3</sup> C/m <sup>2</sup> °C)	0	1.877	0	0

At 10°C, s<sup>IS</sup> = 100 MPa, s<sup>SS</sup> = 80 MPa, e<sub>max</sub><sup>tr</sup> = 0.048. ∂s<sup>IS</sup>/∂θ = ∂s<sup>SS</sup>/∂θ = 8 MPa/°C MPa/°C (Ref. (b))

<sup>a</sup>Dunn, M.D., 1993b;<sup>b</sup>Song, G.Q., Sun, Q.P. and Cherakoui, C., 1999;<sup>c</sup>k<sub>0</sub> = 8.85 × 10<sup>-12</sup> C/Vm<sup>2</sup>**Figure 5** Axial stress vs. axial strain in a hybrid composite consisting of a polymeric matrix and cylindrical SMA and PZT inclusions.

the applied axial stress at the initiation of the forward transformation with an increase in the volume fraction of the PZT inclusions. The applied axial stress at the conclusion of the forward transformation in the SMA also increases with an increase in the volume fraction of the PZT inclusions. However, the macroscopic strain in the composite decreases because of an increase in the stiffness of the composite containing a larger volume fraction of the PZT inclusions. The macroscopic strain of the composite increases with an increase in the volume fraction of the SMA inclusions because of the larger transformation strain induced in the SMA.

**Figure 6** Axial stress vs. axial strain in a hybrid composite consisting of a polymeric matrix and spherical SMA and PZT inclusions.

Results plotted in Figures 5 and 6 also establish that the axial stress vs. the axial strain curves are sensitive to the shapes of the inclusions. Since the spherical SMA inclusions are completely embedded in the softer polymeric matrix, the equivalent stress for the initiation of the forward transformation is reached at a higher value of the applied axial stress than that in the cylindrical SMA inclusions. In general, the stress distribution in the inclusions is such that the equivalent stress or the von Mises stress in the spherical inclusions is larger than that in the cylindrical inclusions for the same value of the applied axial stress. Thus the forward

transformation in the spherical SMA inclusions is completed more quickly than that in the cylindrical SMA inclusions.

We note that most PZTs can withstand a maximum tensile strain of about 0.1 to 0.2%. When all of the SMA and the PZT inclusions are cylindrical, the axial strain induced in each one of them and the matrix will be the same and the axial stresses will be different. Thus, unless new ceramic materials capable of withstanding higher tensile strains become available, the hybrid composite comprised of an elastic matrix and all cylindrical SMA and PZT inclusions can be used only when the PZT is loaded in compression. However, as shown in Figure 7, when the SMA and the PZT inclusions are spherical and the overall axial strain is 3%, the maximum axial strain induced in the PZT is only 0.2% which is within the allowable limits.

Figure 8 exhibits the average axial stress vs. the average axial strain curves for the hybrid composite containing ellipsoidal SMA and cylindrical PZT inclusions with  $f_S = f_P = 0.30$ . Let  $a_1, a_2$  and  $a_3$  denote respectively the principal radii of the ellipsoid along the  $x_1, x_2$  and  $x_3$  axes. Results have been computed for the case of  $a_1 = a_2$  but different values of  $r = a_3/a_1$ ;  $r = \infty$  for cylindrical SMA inclusions and  $r \simeq 0$  for penny shape SMA inclusions. It is clear that for the cylindrical SMA inclusions the axial stress required to induce the phase transformation in the SMA is the least, and for the same applied axial stress the transformation strain produced is the largest of all of the values of  $r$  considered. The area of the hysteresis loop increases with a decrease in the value of  $r$ .

**Stress-Electric Displacement Relations**

Although the response of the PZT material has been modeled as linear, the piezoelectric behavior of the composite is nonlinear because of the forward and the reverse transformations in the SMA inclusions; cf. Figures 9, 10 and 11. Since the spherical PZT inclusions are completely embedded in the polymer matrix which has non-electromechanically coupled properties and low values of the dielectric constants, the electric displacement  $D_3$  induced by the applied axial stress  $\sigma_{33}$  for the hybrid composite with the spherical inclusions is nearly  $10^{-4}$  times that for the cylindrical inclusions. Figures 9, 10 and 11 depict that  $D_3$  varies linearly with  $\sigma_{33}$  both prior to the initiation of the forward transformation and after the completion of the reverse transformation in the SMA. However, when either one of the two transformations is in progress, the magnitude of  $D_3$  changes rapidly with a change in the value of the applied axial stress  $\sigma_{33}$ . For reasons delineated in the previous section, the average applied axial traction at the initiation of the forward transformation in the SMA inclusions decreases with a decrease in the volume fraction of the PZT

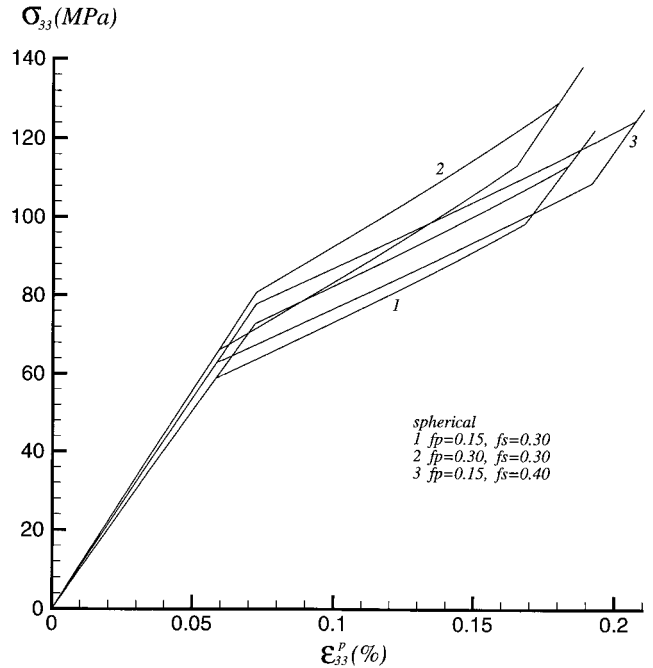


Figure 7. Average axial stress vs. the axial strain in the PZT inclusions for an hybrid composite made of an elastic matrix and spherical PZT and SMA inclusions.

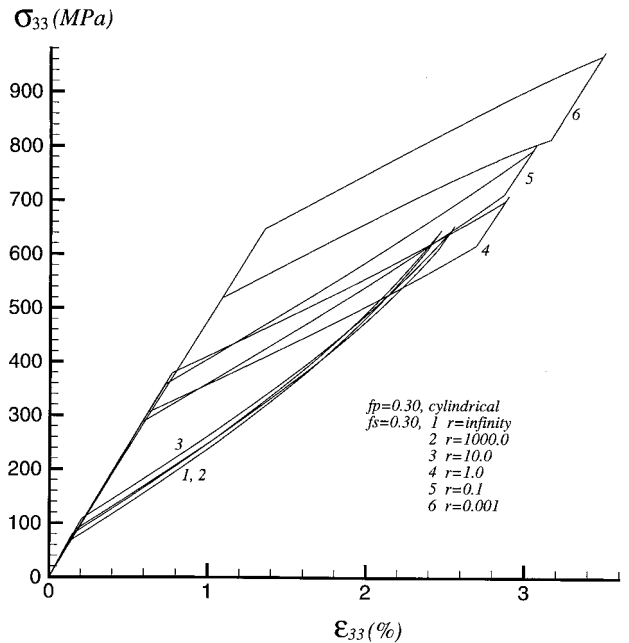
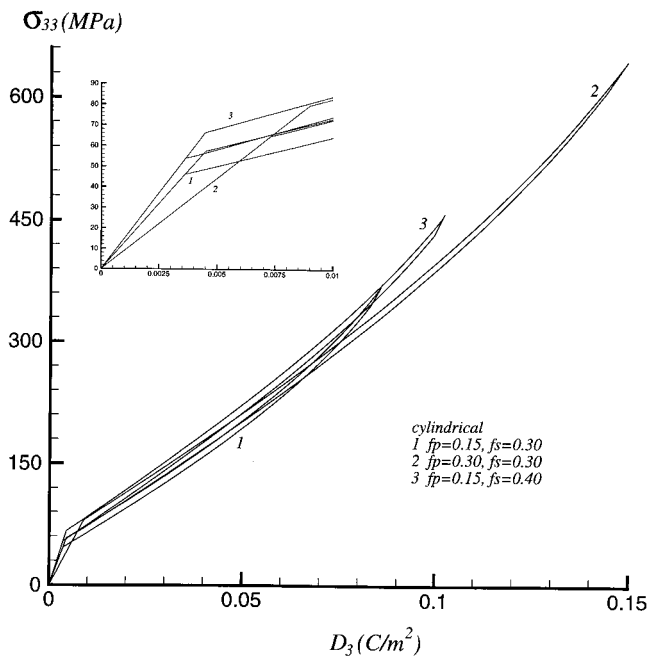
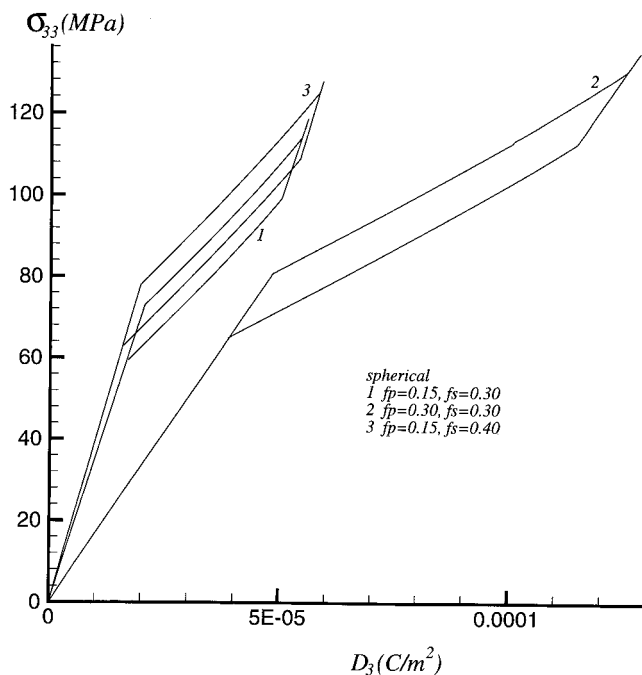


Figure 8. Axial stress vs. axial strain in an hybrid composite consisting of cylindrical PZT inclusions and ellipsoidal SMA inclusions.

inclusions. Thus for the same value of the applied axial stress, the magnitude of the electric displacement  $D_3$  increases with a decrease in the volume fraction of the PZT inclusions because the forward transformation occurs more readily in the SMA inclusions. However, after the conclusion of either the forward or the reverse transformation in the SMA inclusions, the electric



**Figure 9.** Axial stress vs. axial electric displacement for a three-phase composite consisting of a polymeric matrix and cylindrical SMA and PZT inclusions.



**Figure 10.** Axial stress vs. axial electric displacement for a three-phase composite consisting of a polymeric matrix and spherical SMA and PZT inclusions.

displacement of the hybrid composite decreases with a decrease in the volume fraction of the PZT inclusions. Said differently, the phase transformation in the SMA inclusions enhances the electromechanical coupling properties of the composite. For the same volume fraction of the PZT inclusions and the applied axial stress, the magnitude of the axial electric displacement

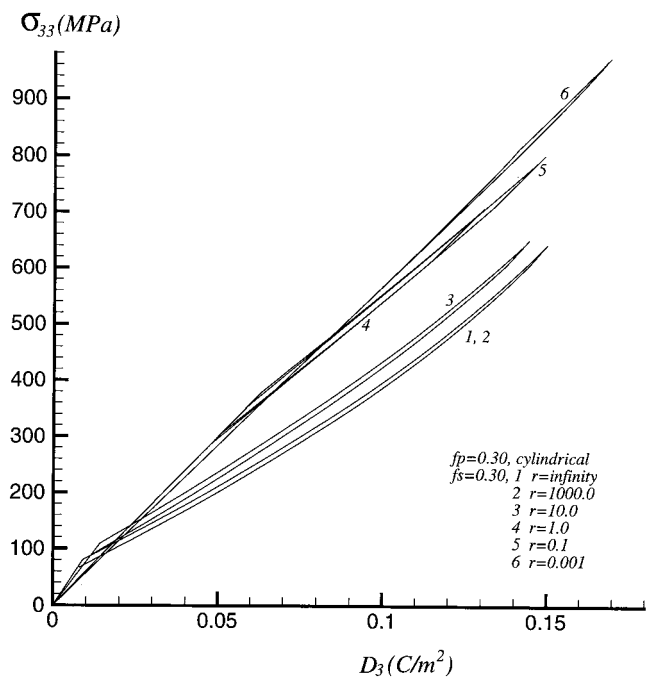


**Figure 11.** Axial stress vs. axial electric displacement for a three-phase composite consisting of a polymeric matrix, cylindrical PZT and ellipsoidal SMA inclusions with  $f_S = f_P = 0.3$ .

decreases with an increase in the volume fraction of the SMA inclusions.

We have plotted in Figure 11 the axial stress vs. the axial electric displacement for the case of the cylindrical PZT and the ellipsoidal SMA inclusions. A comparison of these results with the curve 2 of Figure 9 reveals that for the cylindrical SMA inclusions the axial stress for the same value of the axial electric displacement is the least. The axial stress required to induce the same axial electric displacement increases with a decrease in the value of the aspect ratio  $r$ .

### Effect of the Applied Electric Field

For the case of the spherical PZT inclusions completely embedded in a non-electromechanically coupled polymer matrix with low values of the dielectric constants, the electrical field applied to the hybrid composite to induce a phase transformation in the SMA inclusions is very large. Thus we discuss only the case of the cylindrical PZT inclusions for which Figures 12 and 13 depict the relationship between the applied axial electric field  $E_3$  and the induced axial strain  $\epsilon_{33}$ . Both prior to the initiation and after the conclusion of the phase transformation in the SMA,  $\epsilon_{33}$  varies linearly with  $E_3$ , and, for a fixed value of  $E_3$ , the macroscopic axial strain  $\epsilon_{33}$  increases with an increase in the volume fraction of the PZT inclusions. This is because the axial strain is induced only due to the electromechanical coupling properties of the PZT inclusions. The applied electric field at the initiation of the forward

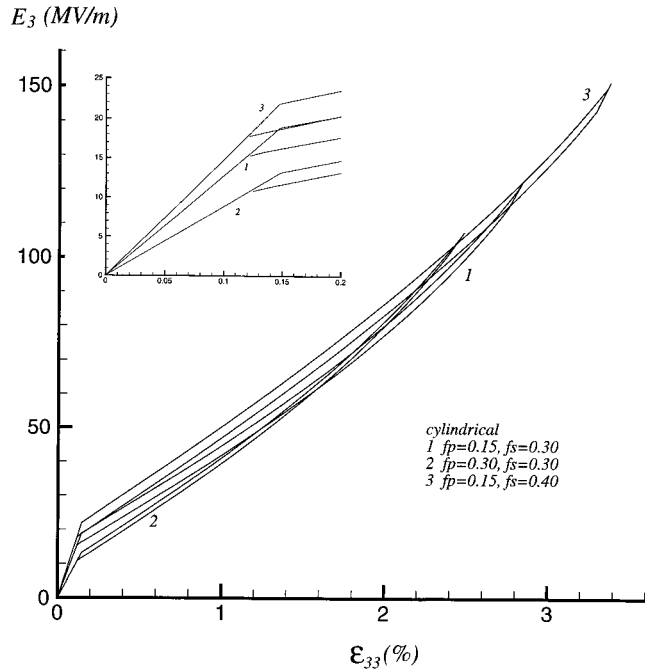


Figure 12. Axial electric field vs. axial strain for a three-phase composite consisting of a polymeric matrix and cylindrical SMA and PZT inclusions.

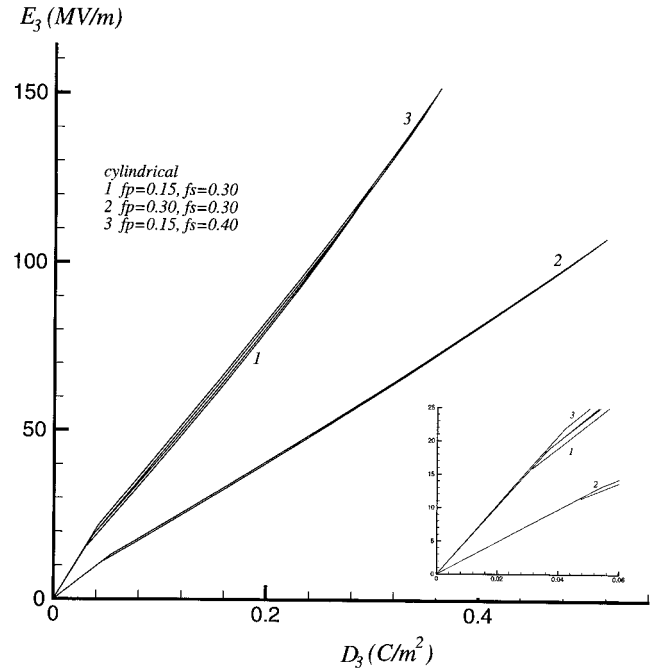


Figure 14. Axial electric field vs. axial electric displacement in a three-phase composite consisting of a polymeric matrix and cylindrical SMA and PZT inclusions.

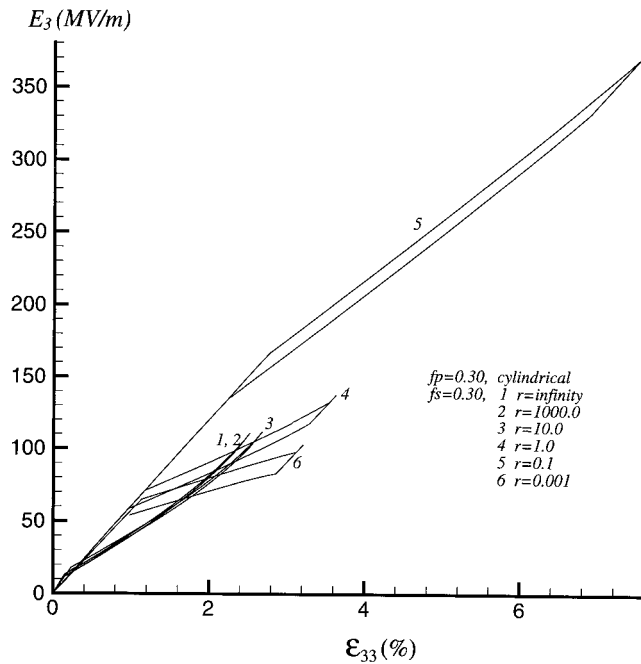


Figure 13. Axial electric field vs. axial strain for a three-phase composite made of a polymeric matrix, cylindrical PZT inclusions and ellipsoidal SMA inclusions with  $f_S = f_P = 0.3$ .

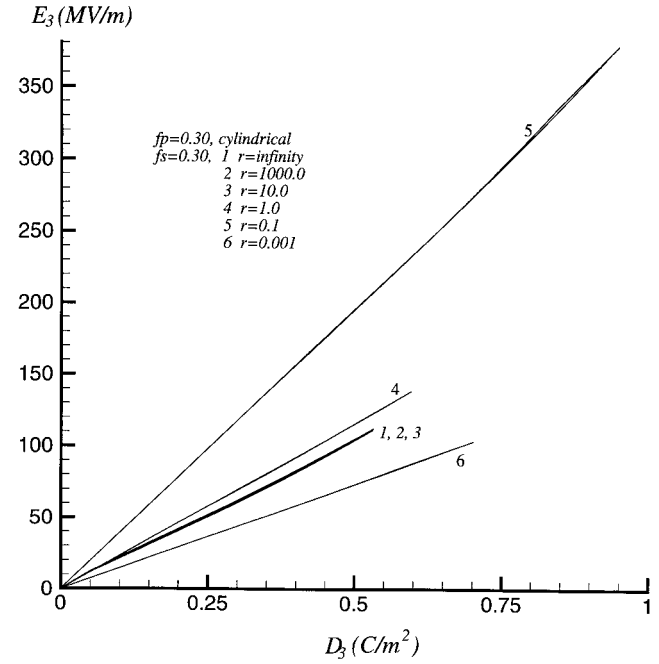


Figure 15. Axial electric field vs. axial electric displacement in a three-phase composite made of a polymeric matrix, cylindrical PZT inclusions, and ellipsoidal SMA inclusions with  $f_S = f_P = 0.3$ .

transformation in the SMA decreases with an increase in the volume fraction of the PZT inclusions, and increases with an increase in the volume fraction of the SMA inclusions. However, as the phase transformation in the SMA progresses, the transformation strain is much larger than the strain induced by the applied electric

field in a pure PZT material and the relation between  $E_3$  and  $\epsilon_{33}$  for the three-phase composite is nonlinear. Results depicted in Figure 13 suggest that for the cylindrical SMA inclusions, the value of the axial electric field at the initiation of the phase transformation in the SMA is the lowest. The area of the ‘‘hysteresis

loop” does not vary monotonically as the value of the aspect ratio,  $r$ , is decreased from  $\infty$  to  $10^{-3}$ , i.e., the shape of the SMA inclusions is changed from cylindrical to penny shape.

Figures 14 and 15 depict the variation of the axial electric displacement  $D_3$  with the applied axial electric field  $E_3$ . The effect of the phase transformation in the SMA inclusions is much less noticeable on these curves. The magnitude of the electric displacement in the hybrid composite increases with an increase in the volume fraction of the PZT inclusions.

Recalling that the dielectric strength of a typical PZT is about 2 MV/m, results plotted in Figures 12 and 13 suggest that it may not be possible to induce large actuation strains just by applying an electric field across the faces of a patch made of the hybrid composite. The

consideration of the electric heat generated by the electric current should facilitate the initiation of the phase transformation in the SMA and will reduce somewhat the required electric field.

**Tabulated Values**

In Tables 2 through 7 we have listed the computed values of the effective electromechanical moduli of the 3-phase composite with the  $x_3$ -axis aligned along the polarization axis of the PZT inclusions. Values listed in Tables 2, 3 and 4 assume that all of the SMA inclusions are in the austenite phase, and those in Tables 5, 6 and 7 are for the case of the SMA inclusions in the martensite phase. It is clear from these results that the effective electroelastic moduli are symmetric when all of the

**Table 2. Values of effective moduli for the 3-phase composite made of polymeric matrix, and cylindrical PZT and SMA inclusions. The SMA material is modeled as austenite.**

	$f_S = 0.15$			$f_S = 0.30$			$f_S = 0.40$		
	$f_P = 0.15$	$f_P = 0.30$	$f_P = 0.40$	$f_P = 0.15$	$f_P = 0.30$	$f_P = 0.40$	$f_P = 0.15$	$f_P = 0.30$	$f_P = 0.40$
$\bar{C}_{1111}$ (GPa)	12.20	15.81	19.36	15.77	21.63	28.10	19.27	28.04	39.09
$\bar{C}_{1122}$ (GPa)	6.40	8.09	9.76	8.18	11.00	14.16	9.96	14.31	19.93
$\bar{C}_{1133}$ (GPa)	6.59	8.27	9.92	8.67	11.54	14.72	10.72	15.18	20.84
$\bar{C}_{3333}$ (GPa)	34.00	50.16	61.28	44.92	61.92	74.10	52.72	70.86	84.78
$\bar{C}_{1212}$ (GPa)	2.90	3.86	4.80	3.80	5.31	6.97	4.66	6.86	9.58
$\bar{C}_{1313}$ (GPa)	3.13	4.31	5.47	4.19	6.02	8.02	5.19	7.82	11.04
$\bar{e}_{311}$ (C/m <sup>2</sup> )	$-6.60 \times 10^{-2}$	-0.163	-0.259	$-8.19 \times 10^{-2}$	-0.215	-0.363	$-9.76 \times 10^{-2}$	-0.273	-0.496
$\bar{e}_{333}$ (C/m <sup>2</sup> )	2.98	5.94	7.89	2.97	5.90	7.81	2.95	5.85	7.72
$\bar{e}_{131}$ (C/m <sup>2</sup> )	$1.02 \times 10^{-3}$	$2.98 \times 10^{-3}$	$5.34 \times 10^{-3}$	$1.08 \times 10^{-3}$	$3.24 \times 10^{-3}$	$6.02 \times 10^{-3}$	$1.16 \times 10^{-3}$	$3.62 \times 10^{-3}$	$7.09 \times 10^{-3}$
$\bar{k}_{11}/k_0$	3.99	5.39	6.63	2.95	3.99	4.87	2.40	3.26	3.98
$\bar{k}_{33}/k_0$	194.66	385.79	513.08	194.05	385.12	512.29	193.64	384.64	511.66
$\bar{\lambda}_{11}$ (MPa/°C)	1.06	1.09	1.12	1.12	1.18	1.24	1.17	1.27	1.39
$\bar{\lambda}_{33}$ (MPa/°C)	1.10	1.09	1.09	1.22	1.23	1.25	1.32	1.35	1.42
$\bar{p}_1$ (C/m <sup>2</sup> °C)	0.00	0.00	0.00	0.00	0.00	0.00	0.00	0.00	0.00
$\bar{p}_3$ (C/m <sup>2</sup> °C)	$2.76 \times 10^{-4}$	$5.53 \times 10^{-4}$	$7.37 \times 10^{-4}$	$2.76 \times 10^{-4}$	$5.54 \times 10^{-4}$	$7.39 \times 10^{-4}$	$2.77 \times 10^{-4}$	$5.547 \times 10^{-4}$	$7.416 \times 10^{-4}$

$k_0 = 8.85 \times 10^{-12}$  pF/m

**Table 3. Values of effective moduli for the 3-phase composite made of a polymeric matrix, and spherical PZT and SMA inclusions. The SMA material is modeled as austenite.**

	$f_S = 0.15$			$f_S = 0.30$			$f_S = 0.40$		
	$f_P = 0.15$	$f_P = 0.30$	$f_P = 0.40$	$f_P = 0.15$	$f_P = 0.30$	$f_P = 0.40$	$f_P = 0.15$	$f_P = 0.30$	$f_P = 0.40$
$\bar{C}_{1111}$ (GPa)	12.94	17.16	21.27	17.07	23.08	31.10	21.07	30.96	43.10
$\bar{C}_{1122}$ (GPa)	6.53	8.33	10.09	8.44	11.43	14.77	10.34	14.95	20.85
$\bar{C}_{1133}$ (GPa)	6.52	8.28	10.01	8.41	11.36	14.62	10.31	14.84	20.61
$\bar{C}_{3333}$ (GPa)	12.98	17.27	21.48	17.13	23.98	31.47	21.14	31.23	43.73
$\bar{C}_{1212}$ (GPa)	3.20	4.42	5.59	4.32	6.18	8.17	5.36	8.01	11.13
$\bar{C}_{1313}$ (GPa)	3.23	4.49	5.73	4.35	6.30	8.42	5.41	8.19	11.54
$\bar{e}_{311}$ (C/m <sup>2</sup> )	$-6.23 \times 10^{-4}$	$-1.83 \times 10^{-3}$	$-3.31 \times 10^{-3}$	$-6.87 \times 10^{-4}$	$-2.08 \times 10^{-3}$	$-3.88 \times 10^{-3}$	$-7.49 \times 10^{-4}$	$-2.34 \times 10^{-3}$	$-4.54 \times 10^{-3}$
$\bar{e}_{333}$ (C/m <sup>2</sup> )	$2.50 \times 10^{-3}$	$7.37 \times 10^{-3}$	$1.34 \times 10^{-2}$	$2.81 \times 10^{-3}$	$8.61 \times 10^{-3}$	$1.63 \times 10^{-2}$	$3.13 \times 10^{-3}$	$1.00 \times 10^{-2}$	$1.996 \times 10^{-2}$
$\bar{e}_{131}$ (C/m <sup>2</sup> )	$1.78 \times 10^{-3}$	$5.25 \times 10^{-3}$	$9.52 \times 10^{-3}$	$1.99 \times 10^{-3}$	$6.10 \times 10^{-3}$	$1.15 \times 10^{-3}$	$2.21 \times 10^{-3}$	$7.05 \times 10^{-3}$	$1.399 \times 10^{-2}$
$\bar{k}_{11}/k_0$	4.96	7.43	9.69	3.98	6.075	7.93	3.41	5.296	6.936
$\bar{k}_{33}/k_0$	4.96	7.44	9.70	3.99	6.082	7.94	3.42	5.301	6.945
$\bar{\lambda}_{11}$ (MPa/°C)	1.07	1.12	1.17	1.14	1.22	1.31	1.20	1.324	1.479
$\bar{\lambda}_{33}$ (MPa/°C)	1.01	0.975	0.94	1.07	1.03	0.997	1.12	1.096	1.077
$\bar{p}_1$ (C/m <sup>2</sup> °C)	0.00	0.00	0.00	0.00	0.00	0.00	0.00	0.00	0.00
$\bar{p}_3$ (C/m <sup>2</sup> °C)	$2.08 \times 10^{-6}$	$4.99 \times 10^{-6}$	$7.68 \times 10^{-6}$	$1.92 \times 10^{-6}$	$4.56 \times 10^{-6}$	$6.95 \times 10^{-6}$	$1.83 \times 10^{-6}$	$4.32 \times 10^{-6}$	$6.559 \times 10^{-6}$

**Table 4. Values of effective moduli for the 3-phase composite made of a polymeric matrix, and cylindrical PZT and spherical SMA inclusions. The SMA material is modeled as austenite.**

	$f_s = 0.15$			$f_s = 0.30$			$f_s = 0.40$		
	$f_p = 0.15$	$f_p = 0.30$	$f_p = 0.40$	$f_p = 0.15$	$f_p = 0.30$	$f_p = 0.40$	$f_p = 0.15$	$f_p = 0.30$	$f_p = 0.40$
$\bar{C}_{1111}$ (GPa)	12.55	16.23	19.84	16.61	22.65	29.28	20.54	29.60	40.89
$\bar{C}_{1122}$ (GPa)	6.47	8.18	9.86	8.36	11.23	14.44	10.25	14.69	20.40
$\bar{C}_{1133}$ (GPa)	6.43	8.07	9.68	8.29	11.04	14.07	10.15	14.35	19.63
$\bar{C}_{3311}$ (GPa)	6.52	8.30	10.04	8.56	11.73	15.23	10.62	15.66	22.00
$\bar{C}_{3333}$ (GPa)	28.14	46.57	59.20	34.45	56.77	72.50	40.22	66.39	85.69
$\bar{C}_{1212}$ (GPa)	3.04	4.03	4.99	4.126	5.71	7.42	5.15	7.45	10.24
$\bar{C}_{1313}$ (GPa)	3.17	4.36	5.52	4.290	6.14	8.16	5.34	7.99	11.23
$\bar{e}_{311}$ (C/m <sup>2</sup> )	$-4.65 \times 10^{-2}$	-0.115	-0.183	$-2.55 \times 10^{-2}$	$-6.70 \times 10^{-2}$	-0.113	$3.30 \times 10^{-3}$	$9.19 \times 10^{-3}$	$1.66 \times 10^{-2}$
$\bar{e}_{333}$ (C/m <sup>2</sup> )	3.44	6.86	9.135	4.05	8.10	10.78	4.61	9.21	12.29
$\bar{e}_{131}$ (C/m <sup>2</sup> )	$1.06 \times 10^{-3}$	$3.13 \times 10^{-3}$	$5.70 \times 10^{-3}$	$1.14 \times 10^{-3}$	$3.50 \times 10^{-3}$	$6.63 \times 10^{-3}$	$1.23 \times 10^{-3}$	$3.94 \times 10^{-3}$	$7.85 \times 10^{-3}$
$\bar{k}_{11}/k_0$	4.32	5.91	7.37	3.39	4.69	5.84	2.85	3.98	4.97
$\bar{k}_{33}/k_0$	181.09	358.93	477.41	168.77	335.06	445.86	161.42	320.85	427.14
$\bar{\lambda}_{11}$ (MPa/°C)	1.06	1.09	1.12	1.12	1.18	1.24	1.18	1.28	1.39
$\bar{\lambda}_{33}$ (MPa/°C)	1.047	1.06	1.076	1.13	1.19	1.25	1.21	1.33	1.45
$\bar{p}_1$ (C/m <sup>2</sup> °C)	0	0	0	0	0	0	0	0	0
$\bar{p}_3$ (C/m <sup>2</sup> °C)	$2.719 \times 10^{-4}$	$5.44 \times 10^{-4}$	$7.26 \times 10^{-4}$	$2.66 \times 10^{-4}$	$5.33 \times 10^{-4}$	$7.11 \times 10^{-4}$	$2.61 \times 10^{-4}$	$5.23 \times 10^{-4}$	$6.79 \times 10^{-4}$

**Table 5. Values of effective moduli for the 3-phase composite made of a polymeric matrix, and cylindrical PZT and SMA inclusions. The SMA material is modeled as martensite.**

	$f_s = 0.15$			$f_s = 0.30$			$f_s = 0.40$		
	$f_p = 0.15$	$f_p = 0.30$	$f_p = 0.40$	$f_p = 0.15$	$f_p = 0.30$	$f_p = 0.40$	$f_p = 0.15$	$f_p = 0.30$	$f_p = 0.40$
$\bar{C}_{1111}$ (GPa)	11.846	15.275	18.605	14.739	19.877	25.363	17.398	24.517	32.888
$\bar{C}_{1122}$ (GPa)	6.308	7.952	9.558	7.887	10.492	13.332	9.393	13.184	17.809
$\bar{C}_{1133}$ (GPa)	6.425	8.026	9.585	8.180	10.725	13.462	9.814	13.495	17.879
$\bar{C}_{3333}$ (GPa)	27.771	43.890	54.947	32.360	49.143	61.014	35.785	53.378	66.409
$\bar{C}_{1212}$ (GPa)	2.769	3.661	4.523	3.426	4.692	6.015	4.002	5.667	7.539
$\bar{C}_{1313}$ (GPa)	2.954	4.039	5.088	3.692	5.195	6.756	4.327	6.258	8.402
$\bar{e}_{311}$ (C/m <sup>2</sup> )	$-6.464 \times 10^{-2}$	-0.1594	-0.252	$-7.793 \times 10^{-2}$	-0.202	-0.335	$-9.030 \times 10^{-2}$	-0.245	-0.430
$\bar{e}_{333}$ (C/m <sup>2</sup> )	2.979	5.939	7.894	2.969	5.907	7.833	2.959	5.874	7.763
$\bar{e}_{131}$ (C/m <sup>2</sup> )	$9.854 \times 10^{-4}$	$2.845 \times 10^{-3}$	$5.066 \times 10^{-3}$	$9.901 \times 10^{-4}$	$2.898 \times 10^{-3}$	$5.247 \times 10^{-3}$	$1.016 \times 10^{-3}$	$3.035 \times 10^{-3}$	$5.632 \times 10^{-3}$
$\bar{k}_{11}/k_0$	3.993	5.393	6.635	2.951	3.987	4.867	2.396	3.262	3.982
$\bar{k}_{33}/k_0$	194.661	385.794	513.094	194.052	385.137	512.344	193.643	384.679	511.774
$\bar{\lambda}_{11}$ (MPa/°C)	1.018	1.038	1.057	1.014	1.038	1.065	1.011	1.039	1.073
$\bar{\lambda}_{33}$ (MPa/°C)	0.983	0.970	0.964	0.9766	0.966	0.9658	0.971	0.964	0.969
$\bar{p}_1$ (C/m <sup>2</sup> °C)	0.00	0.00	0.00	0.00	0.00	0.00	0.00	0.00	0.00
$\bar{p}_3$ (C/m <sup>2</sup> °C)	$2.759 \times 10^{-4}$	$5.520 \times 10^{-4}$	$7.363 \times 10^{-4}$	$2.758 \times 10^{-4}$	$5.520 \times 10^{-4}$	$7.364 \times 10^{-4}$	$2.758 \times 10^{-4}$	$5.520 \times 10^{-4}$	$7.365 \times 10^{-4}$

inclusions are of the same shape, and do not retain the symmetry properties when inclusions are of different shapes. This asymmetry in the material moduli comes from the use of the mean field theory. However, when an energy equivalent method is used to derive the material properties, the effective material moduli are symmetric even when inclusions are of different shapes. When a phase transformation occurs in the SMA phase, approximate values of the effective moduli can be obtained by using the rule of mixtures. We hope that the values provided in these tables will enable researchers in the field to analyze other problems for the 3-phase composite and explore their use as sensors and actuators.

**Remarks**

The heat generated by the electric field and the hysteresis exhibited by the SMA have been neglected. Also, creep effects in the epoxy matrix have been ignored. One way to account for all these effects is to numerically solve an initial-boundary-value problem which is computationally expensive.

**CONCLUSIONS**

Based on the mean field theory and the Mori-Tanaka method, we have derived macroscopic constitutive

**Table 6. Values of effective moduli for the 3-phase composite made of a polymeric matrix, and spherical PZT and SMA inclusions. The SMA material is modeled as martensite.**

	$f_S = 0.15$			$f_S = 0.30$			$f_S = 0.40$		
	$f_P = 0.15$	$f_P = 0.30$	$f_P = 0.40$	$f_P = 0.15$	$f_P = 0.30$	$f_P = 0.40$	$f_P = 0.15$	$f_P = 0.30$	$f_P = 0.40$
$\bar{C}_{1111}$ (GPa)	12.452	16.427	20.247	15.666	21.467	27.541	18.567	26.421	35.385
$\bar{C}_{1122}$ (GPa)	6.434	8.176	9.875	8.117	10.869	13.850	9.714	13.696	18.491
$\bar{C}_{1133}$ (GPa)	6.420	8.136	9.803	8.099	10.814	13.744	9.693	13.626	18.350
$\bar{C}_{3333}$ (GPa)	12.485	16.527	20.430	15.711	21.612	27.827	18.624	26.615	35.797
$\bar{C}_{1212}$ (GPa)	3.009	4.125	5.186	3.775	5.299	6.846	4.426	6.363	8.447
$\bar{C}_{1313}$ (GPa)	3.032	4.193	5.310	3.805	5.395	7.034	4.464	6.489	8.710
$\bar{e}_{311}$ (C/m <sup>2</sup> )	$-5.936 \times 10^{-4}$	$-1.723 \times 10^{-3}$	$-3.083 \times 10^{-3}$	$-6.116 \times 10^{-4}$	$-1.792 \times 10^{-3}$	$-3.233 \times 10^{-3}$	$-6.277 \times 10^{-4}$	$-1.851 \times 10^{-3}$	$-3.353 \times 10^{-3}$
$\bar{e}_{333}$ (C/m <sup>2</sup> )	$2.416 \times 10^{-3}$	$7.062 \times 10^{-3}$	$1.272 \times 10^{-2}$	$2.590 \times 10^{-3}$	$7.746 \times 10^{-3}$	$1.429 \times 10^{-2}$	$2.761 \times 10^{-3}$	$8.468 \times 10^{-3}$	$1.608 \times 10^{-2}$
$\bar{e}_{131}$ (C/m <sup>2</sup> )	$1.715 \times 10^{-3}$	$5.008 \times 10^{-3}$	$9.009 \times 10^{-3}$	$1.825 \times 10^{-3}$	$5.438 \times 10^{-3}$	$9.996 \times 10^{-3}$	$1.931 \times 10^{-3}$	$5.884 \times 10^{-3}$	$1.109 \times 10^{-2}$
$\bar{k}_{11}/k_0$	4.955	7.434	9.689	3.985	6.076	7.928	3.415	5.296	6.936
$\bar{k}_{33}/k_0$	4.958	7.441	9.702	3.987	6.082	7.939	3.417	5.301	6.946
$\bar{\lambda}_{11}$ (MPa/°C)	1.029	1.066	1.100	1.027	1.070	1.115	1.025	1.074	1.129
$\bar{\lambda}_{33}$ (MPa/°C)	0.972	0.926	0.881	0.962	0.904	0.845	0.952	0.884	0.809
$\bar{p}_1$ (C/m <sup>2</sup> °C)	0.00	0.00	0.00	0.00	0.00	0.00	0.00	0.00	0.00
$\bar{p}_3$ (C/m <sup>2</sup> °C)	$2.078 \times 10^{-6}$	$4.990 \times 10^{-6}$	$7.683 \times 10^{-6}$	$1.924 \times 10^{-6}$	$4.562 \times 10^{-6}$	$6.951 \times 10^{-6}$	$1.834 \times 10^{-6}$	$4.320 \times 10^{-6}$	$6.548 \times 10^{-6}$

**Table 7. Values of effective moduli for the 3-phase composite made of a polymeric matrix, and cylindrical PZT and spherical SMA inclusions. The SMA material is modeled as martensite.**

	$f_S = 0.15$			$f_S = 0.30$			$f_S = 0.40$		
	$f_P = 0.15$	$f_P = 0.30$	$f_P = 0.40$	$f_P = 0.15$	$f_P = 0.30$	$f_P = 0.40$	$f_P = 0.15$	$f_P = 0.30$	$f_P = 0.40$
$\bar{C}_{1111}$ (GPa)	12.07	15.51	18.85	15.22	20.37	25.82	18.05	25.14	33.32
$\bar{C}_{1122}$ (GPa)	6.37	8.02	9.64	8.03	10.66	13.50	9.61	13.41	17.99
$\bar{C}_{1133}$ (GPa)	6.32	7.89	9.41	7.94	10.38	12.97	9.46	12.93	16.99
$\bar{C}_{3311}$ (GPa)	6.50	8.35	10.13	8.44	11.68	15.12	10.31	15.21	20.95
$\bar{C}_{3333}$ (GPa)	27.31	45.27	57.59	32.21	53.23	68.05	36.44	60.34	77.85
$\bar{C}_{1212}$ (GPa)	2.85	3.75	4.61	3.59	4.86	6.16	4.22	5.86	7.66
$\bar{C}_{1313}$ (GPa)	2.98	4.06	5.11	3.74	5.24	6.79	4.39	6.31	8.42
$\bar{e}_{311}$ (C/m <sup>2</sup> )	$-2.63 \times 10^{-2}$	$-6.48 \times 10^{-2}$	$-0.102$	$2.55 \times 10^{-2}$	$6.58 \times 10^{-2}$	0.107	$8.33 \times 10^{-2}$	0.225	0.39
$\bar{e}_{333}$ (C/m <sup>2</sup> )	3.35	6.69	8.91	3.81	7.63	10.19	4.21	8.449	11.32
$\bar{e}_{131}$ (C/m <sup>2</sup> )	$1.02 \times 10^{-3}$	$2.99 \times 10^{-3}$	$5.39 \times 10^{-3}$	$1.04 \times 10^{-3}$	$3.12 \times 10^{-3}$	$5.74 \times 10^{-3}$	$1.07 \times 10^{-3}$	$3.282 \times 10^{-3}$	$6.20 \times 10^{-3}$
$\bar{k}_{11}/k_0$	4.32	5.91	7.37	3.39	4.69	5.84	2.85	3.99	4.97
$\bar{k}_{33}/k_0$	181.10	359.00	477.54	168.80	335.21	446.21	161.47	321.10	427.70
$\bar{\lambda}_{11}$ (MPa/°C)	1.02	1.04	1.06	1.014	1.039	1.065	1.011	1.04	1.074
$\bar{\lambda}_{33}$ (MPa/°C)	0.98	0.97	0.96	0.976	0.962	0.961	0.970	0.957	0.962
$\bar{p}_1$ (C/m <sup>2</sup> °C)	0	0	0	0	0	0	0	0	0
$\bar{p}_3$ (C/m <sup>2</sup> °C)	$2.76 \times 10^{-4}$	$5.53 \times 10^{-4}$	$7.37 \times 10^{-4}$	$2.77 \times 10^{-4}$	$5.54 \times 10^{-4}$	$7.383 \times 10^{-4}$	$2.77 \times 10^{-4}$	$5.55 \times 10^{-4}$	$7.39 \times 10^{-4}$

relations for a three phase composite made of PZT and SMA inclusions embedded in a non-electromechanically coupled polymer matrix. All of the PZT inclusions considered are identical in shape and have the same axis of polarization. Similarly, all of the SMA inclusions have the same shape. However, the PZT and SMA inclusions may have different shapes. Because of the transformation strains induced in the SMA inclusions, the hybrid composite exhibits a nonlinear behavior even though the matrix and the PZT are modeled as linear materials. It is found that the cylindrical inclusions are better than the spherical ones in the sense that the applied electric field at the instant of the initiation of the forward transformation in the SMA inclusions is considerably lower for the cylindrical inclusions than that for the spherical inclusions. However, for spherical inclusions, for the same axial stress, the axial strain

induced in the PZTs is considerably less than that in cylindrical inclusions; the latter equals the overall axial strain. Also, the phase transformation in the SMA inclusions is found to enhance the electromechanical coupling properties of the 3-phase composite. The hybrid composite exhibits pyroelectric effect even if none of its constituents is pyroelectric; a similar result was obtained earlier by Dunn (1993b) for a piezo-composite.

A hybrid composite with about 15% PZT and 30% SMA spherical inclusions can make an effective strain gauge since about 3% axial strain is produced by only 100 MPa axial stress.

The macroscopic properties of the hybrid composite provided herein should facilitate the solution of boundary-value problems and the design of such 3-phase sensors and actuators.

## APPENDIX

**Eshelby Tensors for Thermoelastoelectric Deformations**

Consider an ellipsoidal piezoelectric (PZT) inclusion with a uniform eigenstrain  $\epsilon_{ij}^*$  and a uniform eigen-electric field  $E_i^*$  embedded in an infinite nonpiezoelectric but pyroelectric matrix. The constitutive behavior of the PZT inclusion is described by Equation (2), with  $\epsilon_{kl}$  and  $E_k$  replaced by  $\epsilon_{kl} - \epsilon_{kl}^*$  and  $E_k - E_k^*$  respectively, and that of the matrix by Equation (1). In terms of the characteristic function  $h(\mathbf{x})$  defined as

$$h(\mathbf{x}) = \begin{cases} 1 & \text{when } \mathbf{x} \in \Omega_P, \\ 0 & \text{when } \mathbf{x} \notin \Omega_P, \end{cases} \quad (\text{A1})$$

constitutive relations for the PZT and the matrix can be written as

$$\begin{aligned} \sigma_{ij} &= C_{ijkl}^M u_{k,l} - \lambda_{ij}^M \theta + \hat{\sigma}_{ij} h(\mathbf{x}), \\ D_i &= -k_{ij}^M \phi_{,j} + p_i^M \theta + \hat{D}_i h(\mathbf{x}), \end{aligned} \quad (\text{A2})$$

where

$$\begin{aligned} \hat{\sigma}_{ij} &= C_{ijkl}^0 u_{k,l} - \lambda_{ij}^0 \theta + e_{mij}^I (\phi_{,m} + E_m^*) - C_{ijkl}^I \epsilon_{kl}^*, \\ \hat{D}_i &= -k_{im}^0 \phi_{,m} + p_i^0 \theta + e_{ijk}^I (u_{j,k} - \epsilon_{jk}^*) - k_{im}^I E_m^*, \\ \epsilon_{ij} &= (u_{i,j} + u_{j,i})/2, \quad E_i = -\phi_{,i}, \\ C_{ijkl}^0 &= C_{ijkl}^I - C_{ijkl}^M, \quad k_{ij}^0 = k_{ij}^I - k_{ij}^M, \quad \lambda_{ij}^0 = \lambda_{ij}^I - \lambda_{ij}^M, \\ p_i^0 &= p_i^I - p_i^M. \end{aligned} \quad (\text{A3})$$

Here  $\mathbf{u}$  is the mechanical displacement,  $\phi$  the electric potential, and  $\phi_{,i} = \partial\phi/\partial x_i$ ,  $E_i = -\phi_{,i}$ , and the superscript  $I$  refers to the PZT inclusion.

Henceforth we assume that the temperature is uniform throughout the body. In the absence of body forces and free charges, static electroelastoelectric deformations of the PZT and the matrix are governed by

$$\sigma_{ij,j} = 0, \quad D_{i,i} = 0. \quad (\text{A4})$$

Substituting from (A2) into (A4) and recalling that the temperature  $\theta$  is uniform, we arrive at

$$C_{ijkl}^M u_{k,lj} = -[\hat{\sigma}_{ij} h(\mathbf{x})]_{,j}, \quad k_{ij}^M \phi_{,ji} = [\hat{D}_i h(\mathbf{x})]_{,i}. \quad (\text{A5})$$

The terms on the right-hand sides of Equations (A5)<sub>1</sub> and (A5)<sub>2</sub> can be regarded as body forces and distributed charges applied to the matrix. Following Jiang et al. (1997, 1999), the concentration strain  $\epsilon^I$  and the concentration electric field  $\mathbf{E}^I$  in the PZT inclusion can be obtained from

$$\begin{aligned} \epsilon_{ij}^I &= H_{ijkl}^1 \epsilon_{kl}^0 + H_{ijk}^2 E_k^0 + F_{ij}^3 \theta^0 + S_{ijkl}^1 \epsilon_{kl}^* + S_{ijk}^2 E_k^*, \\ E_i^I &= H_{ijk}^3 \epsilon_{jk}^0 + H_{ij}^4 E_j^0 + F_i^2 \theta^0 + S_{ijk}^3 \epsilon_{jk}^* + S_{ij}^4 E_j^*, \end{aligned} \quad (\text{A6})$$

where

$$\begin{aligned} H_{ijkl}^1 &= X_{ijmn} A_{mnkl}, \quad H_{ijk}^2 = X_{ijmn} \alpha_{mnp} B_{pk}, \\ H_{ijk}^3 &= -Y_{im} \beta_{mnp} A_{npj}, \quad H_{ij}^4 = Y_{im} B_{mj}, \\ S_{ijkl}^1 &= I_{ijkl} - X_{ijmn} (I_{mnkl} - \xi_{mnkl}), \\ S_{ijk}^2 &= -X_{ijmn} \alpha_{mnp} (\delta_{pk} - \eta_{pk}), \\ S_{imn}^3 &= Y_{ij} \beta_{jkl} (I_{klmn} - \xi_{klmn}), \\ S_{ij}^4 &= \delta_{ij} - Y_{il} (\delta_{lj} - \eta_{lj}), \\ F_{ij}^1 &= -X_{ijmn} (\chi_{mn} + \alpha_{mnp} \pi_p), \\ F_i^2 &= Y_{ij} (\beta_{jkl} \chi_{kl} - \pi_j), \end{aligned} \quad (\text{A7})$$

are the thermoelastoelectric Eshelby tensors. In Equations (A7),

$$\begin{aligned} A_{ijkl} &= [I_{ijkl} + S_{ijmn}^u (C_{mnpq}^M)^{-1} C_{pqij}^0]^{-1}, \\ B_{ij} &= [\delta_{ij} + S_{im}^\phi (k_{mn}^M)^{-1} k_{nj}^0]^{-1}, \\ \alpha_{ijk} &= Z_{ijmn} e_{kmn}^I, \quad \beta_{ijk} = z_{im} e_{mj}^I, \quad \xi_{ijkl} = Z_{ijmn} C_{mnkl}^I, \\ \eta_{ij} &= z_{im} k_{mj}^I, \quad \chi_{ij} = -Z_{ijmn} \lambda_{mn}^0, \quad \pi_i = z_{ij} p_j^0, \\ X_{ijkl} &= (I_{ijkl} + \alpha_{ijm} \beta_{mkl})^{-1}, \quad Y_{ij} = (\delta_{ij} + \beta_{imn} \alpha_{mnj})^{-1}, \\ Z_{ijkl} &= A_{ijmn} S_{mnpq}^u (C_{pqkl}^M)^{-1}, \quad z_{ij} = B_{im} S_{mn}^\phi (k_{nj}^M)^{-1}, \\ I_{ijkl} &= \frac{1}{2} (\delta_{ik} \delta_{jl} + \delta_{il} \delta_{jk}), \end{aligned} \quad (\text{A8})$$

where  $S^u$  and  $S^\phi$  are respectively the Eshelby tensors for the elastic and the dielectric inclusions whose shapes and orientations are the same as those of the PZT inclusions considered herein. When thermal effects are not considered, i.e.,  $\lambda^P = \mathbf{0}$  and  $\mathbf{p}^P = \mathbf{0}$ , expressions (A7) for the thermoelastoelectric Eshelby tensors reduce to those derived by Jiang et al. (1997). For a nonpiezoelectric inclusion,  $\mathbf{e}^P = \mathbf{0}$ , and expressions (A7) simplify to those of Benveniste and Dvorak (1990). In the space of stress and electric field, we have

$$\begin{aligned} \sigma_{ij}^I &= H_{ijkl}^5 \sigma_{kl}^0 + H_{ijk}^6 E_k^0 + F_{ij}^3 \theta^0 + S_{ijkl}^5 \epsilon_{kl}^* + S_{ijk}^6 E_k^*, \\ E_i^I &= H_{ikl}^7 \sigma_{kl}^0 + H_{ij}^4 E_j^0 + F_i^2 \theta^0 + S_{ikl}^3 \epsilon_{kl}^* + S_{ij}^4 E_j^*, \end{aligned} \quad (\text{A9})$$

where

$$\begin{aligned} H_{ijkl}^5 &= [C_{ijmn}^I H_{mnpq}^1 - e_{mij}^I H_{mpq}^3] (C_{pqkl}^M)^{-1}, \\ H_{ijk}^6 &= C_{ijmn}^I H_{mnk}^2 - e_{mij}^I H_{mk}^4, \\ H_{ijk}^7 &= H_{imn}^3 (C_{mijk}^M)^{-1}, \\ F_{ij}^3 &= C_{ijmn}^I F_{mn}^1 - e_{mij}^I F_m^2 - \lambda_{ij}^I, \\ S_{ijkl}^5 &= C_{ijmn}^I (S_{mnkl}^1 - I_{mnkl}) - e_{mij}^I S_{mkl}^3, \\ S_{ijk}^6 &= C_{ijmn}^I S_{mnk}^2 - e_{mij}^I (S_{mk}^4 - \delta_{mk}). \end{aligned} \quad (\text{A10})$$

For the hybrid composite studied herein, only the SMA inclusion has an eigenstrain, and there is no eigen-electric field in any phase.

### Mori–Tanaka Approximation for Thermoelastoelectric Concentration Tensors

The Mori–Tanaka method approximately accounts for the interaction among inclusions embedded in a matrix. This method gives the following values of the average strain and the average electric field in the matrix.

$$\begin{aligned}\bar{\epsilon}_{ij}^M &= L_{ijkl}^M \epsilon_{kl}^0 + N_{ijk}^M E_k^0 + R_{ij}^M \theta^0 + \epsilon_{ij}^{**M}, \\ \bar{E}_i^M &= P_{ijk}^M \epsilon_{jk}^0 + Q_{ij}^M E_j^0 + J_i^M \theta^0 + E_i^{**M},\end{aligned}\quad (\text{A11})$$

where

$$\begin{aligned}L_{ijkl}^M &= \left[ \mathcal{H}_{ijkl}^1 - \mathcal{H}_{ijm}^2 (\mathcal{H}_{mn}^4)^{-1} \mathcal{H}_{nkl}^3 \right]^{-1}, \\ N_{ijk}^M &= -L_{ijmn}^M \mathcal{H}_{mnp}^2 (\mathcal{H}_{pk}^4)^{-1}, \\ P_{ijk}^M &= -(\mathcal{H}_{im}^4)^{-1} \mathcal{H}_{mpq}^3 L_{pqjk}^M, \\ Q_{ij}^M &= (\mathcal{H}_{im}^4)^{-1} (\delta_{mj} - \mathcal{H}_{mkl}^3 N_{klj}^M), \\ R_{ij}^M &= -\left( L_{ijkl}^M \mathcal{F}_{kl}^1 + N_{ijk}^M \mathcal{F}_k^2 \right), \\ J_i^M &= -\left( P_{imn}^M \mathcal{F}_{mn}^1 + Q_{im}^M \mathcal{F}_m^2 \right), \\ \epsilon_{ij}^{**M} &= -f_S L_{ijkl}^M \langle S_{klmn}^{1S} \epsilon_{mn}^{tr} \rangle_S, \\ E_i^{**M} &= -f_S P_{ikl}^M \langle S_{klmn}^{1S} \epsilon_{mn}^{tr} \rangle_S, \\ \mathcal{H}_{ijkl}^1 &= I_{ijkl} - \sum_{r=S,P} f_r \left[ I_{ijkl} - \langle H_{ijkl}^{1r} \rangle_r \right], \\ \mathcal{H}_{ijk}^2 &= f_P \langle H_{ijk}^{2P} \rangle_P, \\ \mathcal{H}_{ijk}^{3P} &= f_P \langle H_{ijk}^{3P} \rangle_P, \\ \mathcal{H}_{ij}^4 &= \delta_{ij} - \sum_{r=S,P} f_r \left[ \delta_{ij} - \langle H_{ij}^{4r} \rangle_r \right], \\ \mathcal{F}_{ij}^1 &= \sum_{r=S,P} f_r \langle F_{ij}^{1r} \rangle_r, \quad \mathcal{F}_i^2 = \sum_{r=S,P} f_r \langle F_i^{2r} \rangle_r.\end{aligned}\quad (\text{A12})$$

The constraint strain and the constraint electric field in the PZT inclusion ( $r = P$ ) and the SMA inclusion ( $r = S$ ) are given by

$$\begin{aligned}\bar{\epsilon}_{ij}^r &= L_{ijkl}^r \epsilon_{kl}^0 + N_{ijk}^r E_k^0 + R_{ij}^r \theta^0 + \epsilon_{ij}^{**r}, \\ \bar{E}_i^r &= P_{ijk}^r \epsilon_{jk}^0 + Q_{ij}^r E_j^0 + J_i^r \theta^0 + E_i^{**r},\end{aligned}$$

where

$$\begin{aligned}L_{ijkl}^r &= H_{ijmn}^{1r} L_{mnkl}^M + H_{ijm}^{2r} P_{mkl}^M, \\ N_{ijk}^r &= H_{ijmn}^{1r} N_{mnk}^M + H_{ijm}^{2r} Q_{mk}^M,\end{aligned}$$

$$\begin{aligned}P_{ijk}^r &= H_{imn}^{3r} L_{nmjk}^M + H_{im}^{4r} P_{mjk}^M, \\ Q_{ij}^r &= H_{imn}^{3r} N_{mnj}^M + H_{im}^{4r} Q_{mj}^M, \\ R_{ij}^r &= F_{ij}^{1r} + H_{ijmn}^{1r} R_{mn}^M + H_{ijm}^{2r} J_m^M, \\ J_i^r &= F_i^{2r} + H_{imn}^{3r} R_{mn}^M + H_{im}^{4r} J_m^M, \\ \epsilon_{ij}^{**r} &= S_{ijmn}^{1r} \epsilon_{mn}^{*r} + H_{ijm}^{2r} \epsilon_{mn}^{**M} + H_{ijm}^{2r} E_m^{**M}, \\ E_i^{**r} &= H_{imn}^{3r} \epsilon_{mn}^{**M} + H_{im}^{4r} E_m^{**M},\end{aligned}$$

In the space of stress and electric field, we have

$$\begin{aligned}\bar{\sigma}_{ij}^{\sigma} &= L_{ijkl}^{\sigma} \sigma_{kl}^0 + N_{ijk}^{\sigma} E_k^0 + R_{ij}^{\sigma} \theta^0 + \sigma_{ij}^{**\sigma}, \\ \bar{E}_i^{\sigma} &= P_{ikl}^{\sigma} \sigma_{kl}^0 + Q_{ij}^{\sigma} E_j^0 + J_i^{\sigma} \theta^0 + E_i^{**\sigma},\end{aligned}$$

where

$$\begin{aligned}L_{ijkl}^{\sigma} &= \left[ \mathcal{H}_{ijkl}^5 - \mathcal{H}_{ijm}^6 (\mathcal{H}_{mn}^4)^{-1} \mathcal{H}_{nkl}^7 \right]^{-1}, \\ N_{ijk}^{\sigma} &= -L_{ijmn}^{\sigma} \mathcal{H}_{mnp}^6 (\mathcal{H}_{pk}^4)^{-1}, \\ P_{ijk}^{\sigma} &= -(\mathcal{H}_{im}^4)^{-1} \mathcal{H}_{mpq}^7 L_{pqjk}^{\sigma}, \\ Q_{ij}^{\sigma} &= (\mathcal{H}_{im}^4)^{-1} (\delta_{mj} - \mathcal{H}_{mpq}^7 N_{pqj}^{\sigma}), \\ R_{ij}^{\sigma} &= -(L_{ijmn}^{\sigma} \mathcal{F}_{mn}^3 + N_{ijp}^{\sigma} \mathcal{F}_p^2), \\ J_i^{\sigma} &= -(P_{imn}^{\sigma} \mathcal{F}_{mn}^3 + Q_{im}^{\sigma} \mathcal{F}_m^2), \\ \sigma_{ij}^{**\sigma} &= -f_S L_{ijkl}^{\sigma} \langle S_{klmn}^{5S} \epsilon_{mn}^{tr} \rangle_S, \\ E_i^{**\sigma} &= -f_S P_{ikl}^{\sigma} \langle S_{klmn}^{5S} \epsilon_{mn}^{tr} \rangle_S, \\ \mathcal{H}_{ijkl}^5 &= I_{ijkl} - \sum_{r=S,P} f_r \left[ I_{ijkl} - \langle H_{ijkl}^{5r} \rangle_r \right], \\ \mathcal{H}_{ijk}^6 &= f_P \langle H_{ijk}^{6P} \rangle_P, \\ \mathcal{H}_{ijk}^7 &= f_P \langle H_{ijk}^{7P} \rangle_P, \\ \mathcal{F}_{ij}^3 &= \sum_{r=S,P} f_r \langle F_{ij}^{3r} \rangle_r.\end{aligned}$$

### ACKNOWLEDGEMENT

This work was partially supported by the NSF grant CMS9713453 to Virginia Polytechnic Institute and State University.

### REFERENCES

- Armstrong, W. D. and Kino, H. (1995). Martensitic Transformations in a TiNi Fiber Reinforced 6061 Aluminum Matrix Composite. *Journal of Intelligent Material Systems and Structures*, **6**: 809–816.
- Armstrong, W. D. (1996). A One-Dimensional Model of a Shape Memory Alloy Fiber Reinforced Aluminum Metal Matrix Composite. *Journal of Intelligent Material Systems and Structures*, **7**: 448–454.
- Avellaneda, M. and Swart, P. J. (1998). Calculating the Performance of 1–3 Piezoelectric Composite for Hydrophone Applications: An

- Effective Medium Approach. *Journal of the acoustic Society of America*, **103**: 1449–1467.
- Badcock, R. A. and Birt, E. A. (2000). The Use of 0–3 Piezocomposite Embedded Lamb Wave Sensors for Detection of Damage in Advanced Fiber Composites. *Smart Material and Structures*, **9**: 291–297.
- Banno, H. (1983). Recent Developments of Piezoelectric Ceramic Products and Composites of Synthetic Rubber and Piezoelectric Ceramic Particles. *Ferroelectrics*, **50**: 3–12.
- Bekker, A. and Brinson, L. C. (1997). Temperature-Induced Phase Transformation in a Shape Memory Alloy: Phase Diagram Based Kinetics Approach. *Journal of the Mechanics and Physics of Solids*, **45**: 949–988.
- Benveniste, Y. and Dvorak, G. J. (1990). On a Correspondence Between Mechanical and Thermal Effects in Two-Phase Composites. In: Weng, G. J., Taya, M. and Abe, H. (eds.), *Micromechanics and Inhomogeneity, The Toshio Mura Anniversary Volume*. pp. 65–81.
- Benveniste, Y. and Dvorak, G. J. (1992). On Uniform Fields and Universal Relations in Piezoelectric Composites. *Journal of the Mechanics and Physics of Solids*, **40**: 1295–1312.
- Benveniste, Y. (1993a). Universal Relations in Piezoelectric Composites with Eigenstress and Polarization Fields, Part I: Binary Media-Local Fields and Effective Behavior. *ASME Journal of Applied Mechanics*, **60**: 265–269.
- Benveniste, Y. (1993b). Universal Relations in Piezoelectric Composites with Eigenstress and Polarization Fields, Part II: Multiphase Media-Effective Behavior. *ASME Journal of Applied Mechanics*, **60**: 270–275.
- Bidaux, J. E., Bernet, N., Manson, J. A. E. and Gotthardt, R. (1995). Vibration Frequency Control of Polymer Beam Using Embedded Shape-Memory-Alloy Fibers. *J. de Physique IV*, **5**(C8): 1177–1182.
- Birman, V. (1997). Review of Mechanics of Shape Memory Alloy Structures. *Applied Mechanics Review*, **50**: 629–645.
- Boyd, J. G. and Lagoudas, D. C. (1994). Thermomechanical Response of Shape Memory Composites. *Journal of Intelligent Material Systems and Structures*, **5**: 333–346.
- Boyd, J. G. and Lagoudas, D. C. (1996). A Thermodynamical Constitutive Model for Shape Memory Materials. Part I: The Monolithic Shape Memory Alloy. *International Journal of Plasticity*, **12**: 805–842.
- Chan, H. L. W. and Unsworth, J. (1989). Simple Model for Piezoelectric Ceramic/Polymer 1–3 Composites used in Ultrasonic Transducer Applications. *IEEE Trans. on Ultrasonics, Ferroelectrics and Frequency Control*, **36**: 434–441.
- Cherkaoui, M., Sun, Q. P. and Song, G. Q. (2000). Micromechanics Modeling of Composite with Ductile Matrix and Shape Memory Alloy Reinforcement. *International Journal of Solids and Structures*, **37**: 1577–1594.
- Cherkaoui, M., Sun, Q. P. and Song, G. Q. (1998). On the Micromechanics Modeling of Composite with Ductile Matrix and Shape Memory Alloy Reinforcement. *International Journal of Solids and Structures*.
- Chen, T. Y. (1994). Some Exact Relations of Inclusions in Piezoelectric Media. *International Journal of Engineering Science*, **32**: 553–556.
- Deeg, W. F., (1980). The Analysis of Dislocation, Crack and Inclusion Problem in Piezoelectric Solids. PhD Dissertation, Stanford University.
- Dunn, D. L. and Taya, M. (1993). Micromechanics Predictions of the Effective Electroelastic Moduli of Piezoelectric Composites. *International Journal of Solids and Structures*, **30**: 161–175.
- Dunn, M. L. and Taya, M. (1993). An Analysis of Composite Materials Containing Ellipsoidal Piezoelectric Inhomogeneities. *Proceedings of the Royal Society of London, Series A*, **443**: 265–287.
- Dunn, M. D. (1993a). Exact Relations Between the Thermoelastic Moduli of Heterogeneous Materials. *Proceedings of the Royal Society of London A*, **441**: 549–557.
- Dunn, M. D. (1993b). Micromechanics of Coupled Electroelastic Composites: Effective Thermal Expansion and Pyroelectric Coefficients. *Journal of Applied Physics*, **73**(10): 5131–5140.
- Dunn, M. L. (1994). Thermally Induced Fields in Electroelastic Composite Materials: Average Fields and Effective Behavior. *Journal of Engineering Materials and Technology*, **116**: 200–207.
- Dvorak, G. J. (1990). On Uniform Fields in Heterogeneous Media. *Proceedings of the Royal Society of London, A* **431**: 89–110.
- Fischer, D. D., Sun, Q. P. and Tanaka, K. (1996). Transformation-Induced Plasticity (TRIP). *Applied Mechanics Review*, **49**: 317–364.
- Furuya, Y., Sasaki, A. and Taya, M. (1993). Enhanced Mechanical Properties of TiNi Shape Memory Fiber/Al Matrix Composite. *Materials Transactions JIM*, **34**: 224–227.
- Furuya, Y., Shimamoto A. and Taya, M. (1997). Enhancement of Mechanical Properties of TiNi Fiber Composites by Shape Memory Effect. In: Inoue, K., Taya, M. and Shen, S. (eds.), *Proceedings First US-Japan Workshop on Smart Materials and Structures*. University of Washington, Seattle, WA, 4–5 December 1995, TMS-AIME, 65–74.
- Gabbert, U., Kreher, W. and Köppe, H. (1999). Mathematical Modeling and Numerical Simulation of Smart Structures Controlled by Piezoelectric Wafers and Fibers. In: *Proceedings of the EUROMAT '99 Conference*, Munich.
- Hamada, K., Lee, J. H., Mizuuchi, K., Taya, M. and Inoue, K. (1997). Mechanical Properties of Smart Metal Matrix Composite by Shape Memory Effects. *Mat. Res. Soc. Symp. Proc.*, **459**: 143–148.
- Harrison, W.B. (1976). Flexible Piezoelectric Organic Composites. In: Smith, P.L. and Pohanka (eds.), *Proceedings of the Workshop on Sonar Transducer Materials*. National Research Lab, Washington, D.C., 257–268.
- Hwang, J. H. and Yu, J. S. (1994). Electroelastic Eshelby Tensors for an Ellipsoidal Piezoelectric Inclusion. *Composites Engineering*, **4**(11): 1169–1182.
- Jiang, B., Fang, D. N. and Hwang, K. C. (1997). Effective properties of piezocomposites, Part I: Single Inclusion Problem. *Acta Mechanica Sinica*, **13**(4): 347–354.
- Jiang, B., Fang, D. N. and Hwang, K. C. (1999). A Unified Model for the Multiphase Piezocomposites with Ellipsoidal Inclusions. *International Journal of Solids and Structures*, **36**(18): 2707–2733.
- Jonnalagadda, K. and Sottos, N. R. (1995). Influence of Adhesion on Micromechanical Behavior of SMA Composites. *SPIE*, **2442**: 143–151.
- Jonnalagadda, K., Kline, G. E. and Sottos, N. R. (1997). Local Displacement and Local Transfer in Shape Memory Alloy Composites. *Experimental Mechanics*, **37**: 78–86.
- Lagoudas, D. C., Boyd, J. G. and Bo, Z. (1994). Micromechanics of Active Composites with SMA Fibers. *ASME Journal of Engineering Materials and Technology*, **116**: 337–347.
- Lee, J. H., Hamada, K., Mizuuchi, K., Taya, M. and Inoue, K. (1997). Microstructures and Mechanical Properties of 6061 Al Matrix Smart Composite Containing TiNi Shape Memory Alloy Fiber. *Mat. Res. Soc. Symp. Proc.*, **459**: 419–424.
- Liang, C. and Rogers, C. A. (1990). One Dimensional Thermomechanical Constitutive Relations for Shape Memory Materials. *Journal of Intelligent Material Systems and Structures*, **1**: 207–234.
- Lu, Z. K. and Weng, G. J. (1997). Martensitic Transformation and Stress-Strain Relations of Shape Memory Alloy. *Journal of the Mechanics and Physics of Solids*, **45**: 1905–1928.
- Lu, Z. K. and Weng, G. J. (2000). A Two-Level Micromechanical Theory for a Shape-Memory Alloy Reinforced Composite. *International Journal of Plasticity*, **16**: 1289–1307.
- Mori, T. and Tanaka, K. (1973). Average stress in matrix and average elastic energy of materials with misfitting inclusion. *Acta Metallurgica*, **21**: 571–574.
- Müller, I. (1998). Six Lectures on Shape Memory. *CRM Proceedings and Lecture Notes*, **13**: 125–161.
- Nan, C. W. and Weng, G. J. (2000). Influence of Polarization Orientation on the Effective Properties of Piezoelectric Composites. *Journal of Applied Physics*, **88**: 416–423.
- Newnham, R. E., Skinner, D. P. and Cross, L. E. (1978). Connectivity

- and Piezoelectric-Pyroelectric Composites. *Materials in Engineering*, **2**: 93–106.
- Newnham, R. E., Bowen, L. J., Klinker, K. A. and Cross, L. E. (1980). Composite Piezoelectric Transducers. *Materials in Engineering*, **2**: 93–106.
- Patoor, E., Eberhardt, A. and Berveiller, M. (1988). Thermomechanical Behavior of Shape Memory Alloy. *Archives of Mechanics*, **40**: 775–794.
- Pauer, L. A. (1973). Flexible Piezoelectric Material. *IEEE Intl. Conv. Rec.*, 1–5.
- Raniecki, B., Lexcellent, C. and Tanaka, K. (1992). Thermodynamic Models of Pseudoelastic Behavior of Shape Memory Alloys. *Archives of Mechanics*, **44**: 261–284.
- Schulgasser, K. (1992). Relationships Between the Effective Properties of Transversely Isotropic Piezoelectric Composites. *Journal of the Mechanics and Physics of Solids*, **40**(2): 473–479.
- Smith, W. A. (1989). The Role of Piezocomposites in Ultrasonic Transducers. *Proceedings of the IEEE Ultrasonic Symposium*, 755–766.
- Smith, W. A. and Auld, B. A. (1991). Modeling 1–3 Composite Piezoelectrics: Thickness-Mode Oscillations, *IEEE Transactions on Ultrasonics, Ferroelectrics, and Frequency Control*, **38**: 40–47.
- Sottos, N. R., Kline, G. E., Qidwai, M. A. and Lagoudas, D. C. (1996). Analysis of Phase Transformation Fronts in SMA Composites. *SPIE*, **2715**: 27–438.
- Song, G. Q., Sun, Q. P. and Hwang, K. C. (22–25 April, 1997). Micromechanics Constitutive Modelling for Polycrystalline SMA. In: *Proceedings of IUTAM Symposium Variation of Domains and Free-Boundary Problems in Solid Mechanics*. Paris, France.
- Song G. Q., Sun, Q. P. and Cherkaoui, C. (1999). Role of Microstructure in the Thermomechanical Behavior of SMA Composites. *ASME Journal of Engineering Materials and Technology*, **121**: 86–92.
- Stalmans, R., Delaey, L. and Van Humbeeck, J. (1997). Modelling of Adaptive Composite Materials with Embedded Shape Memory Alloy Wires. *Mat. Res. Soc. Symp. Proc.*, **459**: 119–130.
- Sun, Q. P. and Hwang, K. C. (1993). Micromechanics Modelling for the Constitutive Behavior of Polycrystalline Shape Memory Alloys: I. Derivation of General Relations, II. Study of the Individual Phenomena. *Journal of the Mechanics and Physics of Solids*, **41**: 1–33.
- Sun, G. J. and Sun, C. T. (1995). Bending of Shape Memory Alloy Reinforced Composite Beam. *Journal of Materials Sciences*, **30**: 5750–5754.
- Tanaka, K., Kobayashi, S. and Sato, Y. (1986). Thermomechanics of Transformation Pseudoelasticity and Shape Memory Effect in Alloys. *International Journal of Plasticity*, **2**: 59–72.
- Taya, M., Shimamoto, A. and Furuya, Y. (1995). Design of Smart Composites Based on Shape Memory Effect. In: Poursartip, A. and Street, K. (eds.), *Proceedings ICCM-10*. Whistler, BC, Canada, Vol. 275–282.
- Wang, B. (1992). Three-dimensional Analysis of an Ellipsoidal Inclusion in a Piezoelectric Material. *International Journal Solids and Structures*, **29**: 293–308.
- Yamada, Y., Taya, M. and Watanabe, R. (1993). Strengthening of Metal Matrix Composite by Shape Memory Effect. *Materials Transactions, JIM*, **34**: 254–260.